Influence of Solar Activity Cycles on Earth's Climate

Task 1 – Literature Study

WP 104 – Modelling of Sun-induced Climate Variability

Joanna D. Haigh
Imperial College London

01 August 2005

Contents

1. Climate modelling 3
2. Fluid dynamics 3
   2.1. Equations of motion 3
      2.1.1. Continuity Equation 3
      2.1.2. Equation of state 3
      2.1.3. Thermodynamic equation 4
      2.1.4. Momentum equation 4
   2.2. Representation in climate models 4
      2.2.1. Model grids and discretisation 5
      2.2.2. Turbulence 6
      2.2.3. Models of reduced complexity 7
3. Clouds 7
   3.1. Cloud Formation 7
      3.1.1. Large scale processes 7
      3.1.2. Microphysical processes 8
      3.1.3. Modulation of cloud condensation nucleus concentrations by cosmic rays 8
      3.1.4. Effects of varying electric field on ice cloud processes 9
   3.2. Cloud prediction in models 10
4. Radiative processes 11
   4.1. Earth Radiation Budget 11
   4.2. Radiative transfer 12
      4.2.1. Absorption of solar radiation by the atmosphere 13
      4.2.2. Infrared radiative transfer and the atmospheric temperature structure 15
      4.2.3. Scattering of radiation 17
      4.2.4. Drop size and optical depth 18
   4.3. Radiation schemes in climate models 18
5. Photochemistry 19
   5.1. Stratosphere 19
   5.2. Troposphere 21
6. Modes of variability in the atmosphere 21
   6.1. Modes of variability 21
      6.1.1. The North Atlantic Oscillation 21
      6.1.2. The El Niño-Southern Oscillation 22
      6.1.3. The Quasi-Biennial Oscillation 23
   6.2. Representation in climate models 24
7. Solar variability and climate modelling 25
   7.1. Radiative heating 25
   7.2. Temperatures 28
   7.3. Photochemistry 30
   7.4. Clouds 31
   7.5. Modes of variability 32
8. Conclusions 33
References 33

1. Climate modelling

The aim of this report is to review the role of climate modelling in the advancement of understanding of the effects of solar variability on climate. Global Climate Models (GCMs), which are computer simulations of the state of the atmosphere-ocean system and its variability, have become increasingly important as tools of the climate scientist. Using numerical representations of processes involved, GCMs enable studies of complex interactions within the climate system, their evolution and sensitivity to internal or external forcing factors.

In this report are considered the fundamental physical and chemical processes that need to be included, how they are represented, some of the approximations made and to what extent GCMs are able to reproduce observed signals of solar variability in the atmosphere.

2. Fluid dynamics

2.1. Equations of motion

The atmosphere is a continuous, compressible fluid resting on the surface of a rotating planet. By applying some of the basic laws of physics - conservation of energy, conservation of mass, Newton's 2nd law of motion and the ideal gas law – to this fluid we can acquire an understanding of the main features of the global atmospheric circulation.

2.1.1. Continuity Equation

Consider the flow of air through an elemental volume. The local density, ρ, will increase if mass converges within the volume. Thus the rate of change of density with time is given by:

$$\frac{\partial \rho}{\partial t} = -\nabla.(\rho \boldsymbol{u}) \qquad (2.1)$$

where $\boldsymbol{u}$ is the local velocity (bold type indicates vector variables) and the right-hand-side of the equation represents the divergence of the flux of mass crossing unit area in the direction of $\boldsymbol{u}$.

An alternative way to write this equation is:

$$\frac{1}{\rho}\frac{D\rho}{Dt} + \nabla.\boldsymbol{u} = 0 \qquad (2.2)$$

where the material derivative:

$$\frac{D}{Dt} \equiv \frac{\partial}{\partial t} + \boldsymbol{u}.\nabla \qquad (2.3)$$

represents the rate of change with time following the motion, contrasting with $\frac{\partial}{\partial t}$ which represents the rate of change at a fixed point in space. The former approach, following air parcels, is often referred to as the Lagrangian method.

2.1.2. Equation of state

Assuming that air under normal atmospheric conditions can be treated as an ideal gas (an assumption which is sufficiently accurate where water vapour is not condensing into cloud) we can write:

$$pM = \rho RT \qquad (2.4)$$

where p is atmospheric pressure, M the molecular weight, R the universal gas constant and T temperature.

2.1.3. Thermodynamic equation

Applying the First Law of Thermodynamics to our parcel of air, again using the Lagrangian approach, we find:

$$\frac{DT}{Dt} = Q + \frac{1}{\rho C_p}\frac{Dp}{Dt} \qquad (2.5)$$

where the second term on the right-hand-side represents adiabatic warming/cooling due to compression/expansion and Q is the heating rate due to diabatic factors: mainly radiative processes in the stratosphere and latent heating/cooling in the troposphere.

2.1.4. Momentum equation

Newton's second law of motion states that the acceleration of a body is equal to the ratio of the net force acting on it to its mass. Applying this to a parcel of air we can write:

$$\frac{D\boldsymbol{u}}{Dt} = -g\boldsymbol{k} - \frac{1}{\rho}\nabla p + \frac{\eta}{\rho}\nabla^2\boldsymbol{u} \qquad (2.6)$$

where the terms on the right-hand-side represent the forces per unit mass due to gravity, pressure gradients and friction (viscous drag). $\boldsymbol{k}$ is the unit vector in the vertical direction and η the dynamic viscosity. This equation, however, only applies in an inertial frame of reference (i.e. one which itself is not subject to external forces) and thus needs modification for use in a rotating frame of reference, such as a coordinate system fixed relative to the Earth. In a frame rotating with angular velocity $\boldsymbol{\Omega}$ the equation becomes:

$$\frac{D\boldsymbol{u}}{Dt} + 2\boldsymbol{\Omega}\times\boldsymbol{u} + \boldsymbol{\Omega}\times(\boldsymbol{\Omega}\times r) = -g\boldsymbol{k} - \frac{1}{\rho}\nabla p + \frac{\eta}{\rho}\nabla^2\boldsymbol{u} \qquad (2.7)$$

where the second and third terms are the Coriolis and centripetal accelerations respectively. The centripetal term is small in the atmosphere but acts to distort the shape of the solid Earth from spherical to bulging at the equator. Thus it is usual to incorporate this term in with gravity by defining:

$$\boldsymbol{g}' = -g\boldsymbol{k} - \boldsymbol{\Omega}\times(\boldsymbol{\Omega}\times r) \qquad (2.8)$$

where the effective gravity, vector $\boldsymbol{g}'$, is perpendicular to the local surface of the Earth. Thus the momentum equation becomes:

$$\frac{D\boldsymbol{u}}{Dt} = -2\boldsymbol{\Omega}\times\boldsymbol{u} + \boldsymbol{g}' - \frac{1}{\rho}\nabla p + \frac{\eta}{\rho}\nabla^2\boldsymbol{u} \qquad (2.9)$$

For a comprehensive discussion of the equations of motion see e.g. Holton (1992).

2.2. Representation in climate models

Global Climate Models (GCMs) simulate the state and evolution of the atmosphere through solving the equations of motion at all points on a grid discretised in space and time. The starting point, considering first only dry air, are equations (2.2), (2.4), (2.5) and (2.9) which provide 6 equations for 6 unknowns, *viz* $\boldsymbol{u}$ (three components), p, ρ and T. Given initial and boundary conditions, some properties of dry air (M, C_p, η) and, importantly, a grid of values of the diabatic heating rate Q the equations can be solved in space and iterated in time to produce 4-dimensional fields of the variables. There are, however, a number of complications that make this procedure somewhat less simple than it may first appear:

1. The specification of Q depends on model state. This requires that the radiative transfer equation be solved as a function of the model fields of temperature and composition at each time-step (see section 4).
2. The presence of water is fundamental to the state of the atmosphere providing sources/sinks of latent heat and clouds which have a huge impact on Q. Thus water vapour has to be transported within the model and a scheme to represent convection and condensation needs to be included (see section 3).
3. The discretisation is space and time results in rounding errors and also, possibly, numerically unstable solutions (see section 2.2.1).
4. Some representations need to be included for factors which occur on scales smaller than the grid size but nevertheless impact the large scale, for example surface orography and turbulence (see section 2.2.2).
5. Constraints on computer resources (processing speed, memory, storage) place limitations on what is possible, requiring compromises to be made in grid resolution and/or the detailed representation of particular processes (see section 2.2.3).

2.2.1. Model grids and discretisation

The equations of motion cannot be solved analytically so numerical techniques need to be employed. Approximate solutions can be found using finite difference or series expansion methods in which the continuous functions of the variables are replaced by values on a finite number of spatial and/or temporal nodes (see e.g. Jacobson, 1999). The finite difference approach involves mapping the variables onto a grid and replacing the differential operator, ∂, by a discrete difference, Δ. There is no unique way of accomplishing this and the choice of approximation will depend on requirements with regard to accuracy, stability and convergence for the equation(s) in question. Some examples of low order approximations are given in Table 1.

Table 1 Examples of low order finite difference approximations for $\partial f / \partial x$ and $\partial^2 f / \partial x^2$. The grid-spacing is Δx, the suffix *i* refers to the point at which the differential is being calculated, *i-1* to the point one grid-space in the negative *x*-direction etc.

Order	Approximation
1st order backward	$\partial f_i / \partial x \approx (f_i - f_{i-1}) / \Delta x$
1st order forward	$\partial f_i / \partial x \approx (f_{i+1} - f_i) / \Delta x$
2nd order backward	$\partial f_i / \partial x \approx (3f_i - 4f_{i-1} + f_{i-2}) / 2\Delta x$
2nd order central	$\partial f_i / \partial x \approx (f_{i+1} - f_{i-1}) / 2\Delta x$
2nd order forward	$\partial f_i / \partial x \approx (-f_{i+2} + 4f_{i+1} - 3f_i) / 2\Delta x$
2nd order central	$\partial^2 f_i / \partial x^2 \approx (f_{i+1} - 2f_i + f_{i-1}) / \Delta x^2$
4th order central	$\partial^2 f_i / \partial x^2 \approx (-f_{i+2} + 16f_{i+1} - 30f_i + 16f_{i-1} - f_{i-2}) / 12\Delta x^2$

Numerous schemes have been constructed using various combinations of approximations for the time and space differentials. Higher order approximations tend to be more stable but to smooth out fine structure in the fields. The stability of a scheme also depends on the grid-spacing; for example, the finite difference form of the advection equation tends to become unstable if the timestep is greater than the ratio of the gridlength to the maximum speed (i.e. the shortest time taken to cross a gridbox).

One state-of-the-art GCM which uses finite-differencing is the UK Met Office Unified Model. Figure 2.1 shows how the increase in computer power over the past 47 years has allowed the resolution used in the operational (numerical weather prediction) models to increase (a) the number of model levels and (b) the horizontal resolution. Much of the increase in computer power is also utilised in processing additional data, the quantity of

which has grown in relation to the ability of supercomputers to handle it. In particular, satellite data have become numerous and are increasingly important in shaping the computer-model analysis, especially in areas where there are few other forms of observation. In climate mode the model is typically run on a 130km grid with 19 levels in the vertical up to an altitude of 10hPa and fully coupled to an ocean model. However, different versions are available for particular studies, including one with 64 levels (up to the lower thermosphere) for middle atmosphere studies.

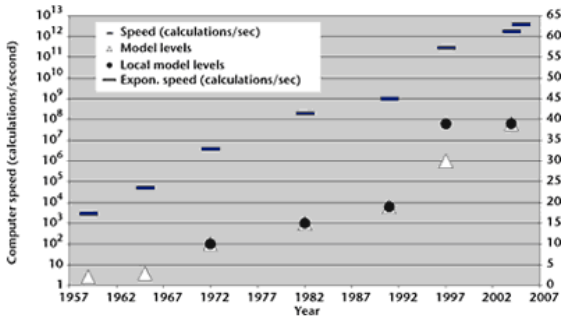

Figure 2.1(a). The processing speed of Met Office computers from 1959 to 2005 has been exponential. The operational model currently runs on a 65-km global grid with 30 levels. The embedded mesoscale grid has 12 km resolution and 39 levels.

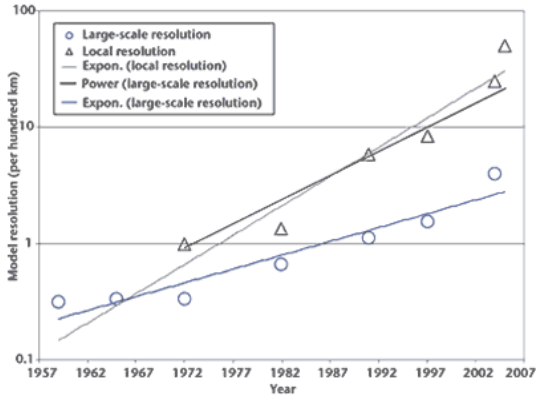

Figure 2.1(b). Met Office model resolution (grid length^{-1}) has decreased markedly since 1959. From http://www.metoffice.com/research/nwp/publications/nwp_gazette/sep02/index.html.

Series expansion methods involve the representation of variables in terms of a finite sum of basis functions which can be defined locally (as in finite element methods) or on model domain scale (as in spectral methods). For global modelling the basis functions are usually spherical harmonics in the horizontal, with finite differences being retained in the vertical and temporal dimensions. These spectral models have the advantage that horizontal differentials can be calculated explicitly and they can be faster computationally. However, they require a continuous switching between spectral space (for the "dynamics") and gridpoint space (for the "physics"). A leading model of this variety is the one developed at the European Centre for Medium Range Weather Forecasting and adapted for climate studies by various establishments including the Max Planck Institut für Meteorologie, Hamburg, where it is known as the ECHAM model. A typical horizontal resolution for a spectral model in climate mode would be given by truncation of the series at horizontal wavenumber 42.

2.2.2. Turbulence

At the surface of the Earth the air flow is necessarily zero but in a thin (50-300m) layer above the surface wind speeds increase logarithmically with height creating a shear layer. This wind shear produces eddies, on all scales up from the molecular, which result in the turbulent transfer of heat and momentum both horizontally and vertically. Surface obstacles such as rocks, trees, buildings also give rise to wind shear and turbulence while surface heating causes thermal turbulence and convection throughout the atmospheric boundary layer (extending up to between 0.5 and 3km). Clearly it is not possible for a model with a horizontal grid spacing of hundreds of kilometres and a vertical resolution of a few kilometres to simulate the details of these eddies but some representation needs to be included of their bulk effect on the momentum and heat budgets. This is usually done using a tensor **K** of eddy diffusion coefficients so, for example, the momentum equation (2.9) will include an additional term: $-\frac{1}{\rho}(\nabla.\rho\mathbf{K}\nabla)\boldsymbol{u}$ where the eddy diffusion coefficients can be specified as functions of

location and season or determined as a function of model state (e.g. wind shear, static stability). This approach is also sometimes used at the top of a model domain, not so as to represent any physical process but merely to ensure that high wind speeds do not develop near the upper boundary.

2.2.3. Models of reduced complexity

Due to computational constraints it is never feasible to include the best possible representations of all the known relevant physical and chemical processes in a GCM. It may not even be desirable – sometimes interpreting GCM output is almost as difficult as interpreting data from the real atmosphere. Under such circumstances it is often more useful to use simplified models which focus on one (or more) aspects of a problem at the expense of the treatment of other features which are deemed to be less important in the particular context.

A common approach is to reduce the dimensionality of the model, at the expense of a complete representation of dynamical processes. For example, 2D (latitude-height) models, in which zonal mean quantities are considered, have been successfully used in studies of stratospheric photochemistry and radiative transfer, including the response to solar variability (see e.g. Haigh, 1994). 1D (height only) Energy Balance Models, which have no transport apart from vertical diffusion, can provide a useful first order estimate of global mean response to radiative forcing perturbations (see section 7.1).

Alternatively, if the focus of attention is on a process occurring in a particular region of the atmosphere, it may be useful to restrict the spatial extent of the model, although care must then be taken with boundary conditions. Some interesting work on links between solar variability, the QBO and polar stratospheric temperatures has been carried out with a model in which the lower boundary was set at the tropopause, thus avoiding the necessity to simulate the complex cloud-radiation and boundary layer effects within the troposphere and allowing long integrations to take place (Gray et al, 2005).

Another approach is to simplify the treatment of certain processes in order to focus on others. For example, studies of coupling between the tropical lower stratosphere and tropospheric circulations, aimed at investigating potential solar amplification mechanisms, have been carried out by Haigh et al (2005) using a model in which all diabatic processes have been reduced to Newtonian relaxation to a reference equilibrium temperature (see section 4.3). This maintains the full representation of dynamical processes but avoids the necessity for detailed calculations of Q thus allowing numerous experiments to be carried out.

3. Clouds

Clouds have a major impact on the heat and radiation budgets of the atmosphere. They transport latent heat from the oceans to the atmosphere. They reflect solar radiation back to space, reducing the net incoming radiative flux, and they trap infrared radiation, acting in a similar way to greenhouse gases. The magnitudes of these effects depends on the location, altitude, time of year and also the physical properties of the cloud. Here we consider how clouds are formed and how their radiative properties relate to their microphysical structure. A short discussion of how clouds are represented in GCMs completes the section.

3.1. Cloud Formation

3.1.1. Large scale processes

Clouds form when the water vapour in the air condenses. Generally this occurs in airmasses which are rising as these expand due to the reduction in pressure and therefore cool

adiabatically. The cooler air has a lower saturated vapour pressure so that the airmass, with a given humidity, becomes saturated. Air masses rise either due to convection or through being forced to pass over some sort of barrier.

Convection takes place when air at the surface is heated. This can be due either to the ground being warmed by the sun or when cool air flows over a warmer surface. The warmed air becomes less dense than that of the surrounding air and starts to rise and cool; at some height (called the condensation level) the air becomes saturated and cloud forms. Within the cloud the decrease of temperature with height is generally less than that of clear air so the ascending volumes remain warmer and more buoyant than the surrounding air. Convective clouds appear as fluffy white heaps but given enough energy can develop into deep storm clouds, reaching the tropopause where the wind blows ice "anvils" off the tops.
Forced ascent may take place over surface topography (hills and mountains) or over other bodies of air. An example of the latter occurs in mid-latitude cyclonic systems which are formed when polar and sub-tropical airmasses collide, creating weather fronts and forcing the warmer air to ride over the colder.

3.1.2. Microphysical processes

Cooling the air to saturation point is not, however, a sufficient condition for cloud to form. In fact it is possible for relative humidities to reach values up to 500 % without any condensation having taken place. In practice the water vapour requires a suitable surface, called a condensation nucleus, on which to condense. If the condensation nucleus is not a water surface then heterogeneous nucleation is said to take place; if it is then homogeneous nucleation occurs. In the free atmosphere, however, heterogeneous nucleation is the only important process because homogeneous nucleation requires prohibitively high relative humidities. (For a comprehensive discussion of cloud formation see the classic text by Ludlam, 1980).

Particles which act as condensation nuclei include sea salt, sulphates, mineral dust and aerosols produced from biomass burning. The concentration and composition of atmospheric aerosol vary geographically with, for example, sulphate aerosol being more abundant in the northern hemisphere as it is generated in industrial regions. A region with a higher concentration of condensation nuclei will produce a larger number of smaller cloud droplets than a remote area with clean air which will produce fewer larger droplets for the same total water content. Smaller drops are more effective at scattering radiation (see section 4.2.4) so that the cloud produced in the air with more aerosol has a higher albedo.

3.1.3. Modulation of cloud condensation nucleus concentrations by cosmic rays

It has been proposed, originally by Dickinson (1975) who acknowledged that his idea was entirely speculative at the time, that variations in cosmic rays could provide a mechanism whereby solar activity would produce a direct impact on cloud cover by modulating atmospheric ionization, resulting in the electrification of aerosol and increasing the effectiveness of this aerosol to act as condensation nuclei. Other processes whereby changes in the Earth's electric field might modify cloud cover, or cloud properties, have also been proposed (see e.g. Tinsley, 2000). The processes involved are complex but if they do take place then there is scope for considerable amendment to the value for solar radiative forcing of climate based on incident irradiance alone.

The mechanism proposed by Dickinson and adopted by Marsh & Svensmark (2000) to account for the correlation of tropical marine low cloud cover and cosmic radiation requires

that modulation by solar variability of cosmic rays causes a response in the concentration of cloud condensation nuclei. Several consecutive processes (summarized in Figure 3.1) need to take place in order for this to come about. Firstly air ions are produced by the action of cosmic rays; this is not controversial, as discussed above, but it should be noted that these ions cannot act directly as cloud condensation nuclei as their small size would require the surrounding air to have a very high level of supersaturation which does not occur in the atmosphere.

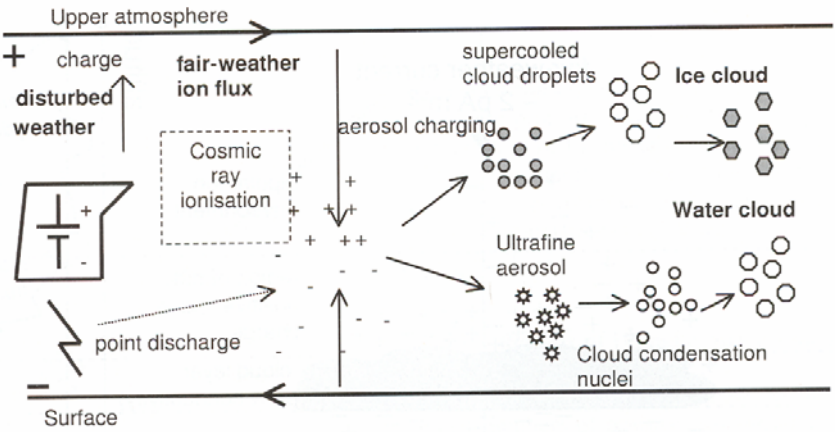

Figure 3.1 Stages in process whereby atmospheric ionisation results in the formation of cloud droplets/crystals. (Harrison and Carslaw, 2003).

The air ions produced by the cosmic rays may act as sites for the nucleation of new ultrafine aerosol (or condensation nuclei, CN). The mechanism then hinges on the extent to which these CN may grow into particles large enough (>~80 nm) to become cloud condensation nuclei (CCN) and whether this process is enhanced by the particles being charged. Growth may occur through condensation of water vapour or other soluble gases or through coagulation among neutral and charged particles. Some observational evidence (Yu and Turco, 2000) suggests that charged molecular clusters grow faster than neutral clusters and chemical box models (Yu and Turco, 2001) have been able to simulate this effect. However, to reach CCN size would take several days and whether the growth can be maintained depends on the supply of vapour and competitive sources of new aerosol and CCN all of which vary with location, altitude and time of year. Yu (2002) suggests that conditions in the lower troposphere may be more favourable than at higher altitudes.

Even if by such a mechanism it proves feasible to produce a measurable effect on cloud cover or properties, the magnitude, and even the sign, of the impact on radiative forcing remains uncertain as it will depend on the cloud location, altitude and physical properties.

3.1.4. Effects of varying electric field on ice cloud processes

At temperatures between -40°C and 0°C liquid water cannot freeze spontaneously by homogeneous nucleation but requires nuclei on which to start freezing. However, only a small proportion of atmospheric aerosol form suitable sites. It has been observed in laboratory experiments that imposition of a large electric field can cause the freezing of supercooled water droplets. Other work has shown that particles which are usually poor ice nuclei became much more efficient when electrically charged. Such processes are collectively known as electrofreezing. In a series of papers Brian Tinsley and co-workers have proposed that solar modulation of cosmic ray ionization may affect electrofreezing processes. The latent heat released during freezing is available for modifying the weather systems of which the ice cloud is a part. This hypothesis awaits confirmation that electrofreezing processes really do take place in the atmosphere and also that the latent heat released is sufficient to produce the apparent effects on cyclone development.

3.2. Cloud prediction in models

Uncertainties and approximations in the representation of cloud formation and cloud radiative properties remain a major cause of uncertainty in current climate prediction models. As discussed above, cloud formation depends on factors ranging from local topography, large scale flow and the temperature and humidity of air masses to the microphysical composition of particulates in the atmosphere. With grid sizes of the order of 100km in the horizontal and 1km in the vertical, there is no possibility of GCMs being able to reproduce realistic cloud structures down to convective scale so they include a variety of parameterisations for cloud prediction.

These schemes include methods for predicting the occurrence of cloud and precipitation and for representing the effects of sub-gridscale convection. There are many varieties of cloud prediction scheme; the simplest estimates high, medium, low and convective cloud cover based on empirical relationships between cloud, relative humidity and vertical velocity (e.g. Slingo 1987) and diagnose precipitation from cloud water (or ice) only. It is necessary also to include the effects of sub-gridscale convection because without these, averaged over a grid box, vertical velocities would be too slow to produce realistic transport of moisture, condensation and latent heat release. The convection schemes parameterize the vigorous vertical transports carried out by updrafts and downdrafts associated with individual clouds. Figure 3.2 indicates some of the processes that need to be included. Numerous assumptions are made in convection schemes which are adjusted to optimize the scheme's overall performance so that they may work well in some situations and not others.

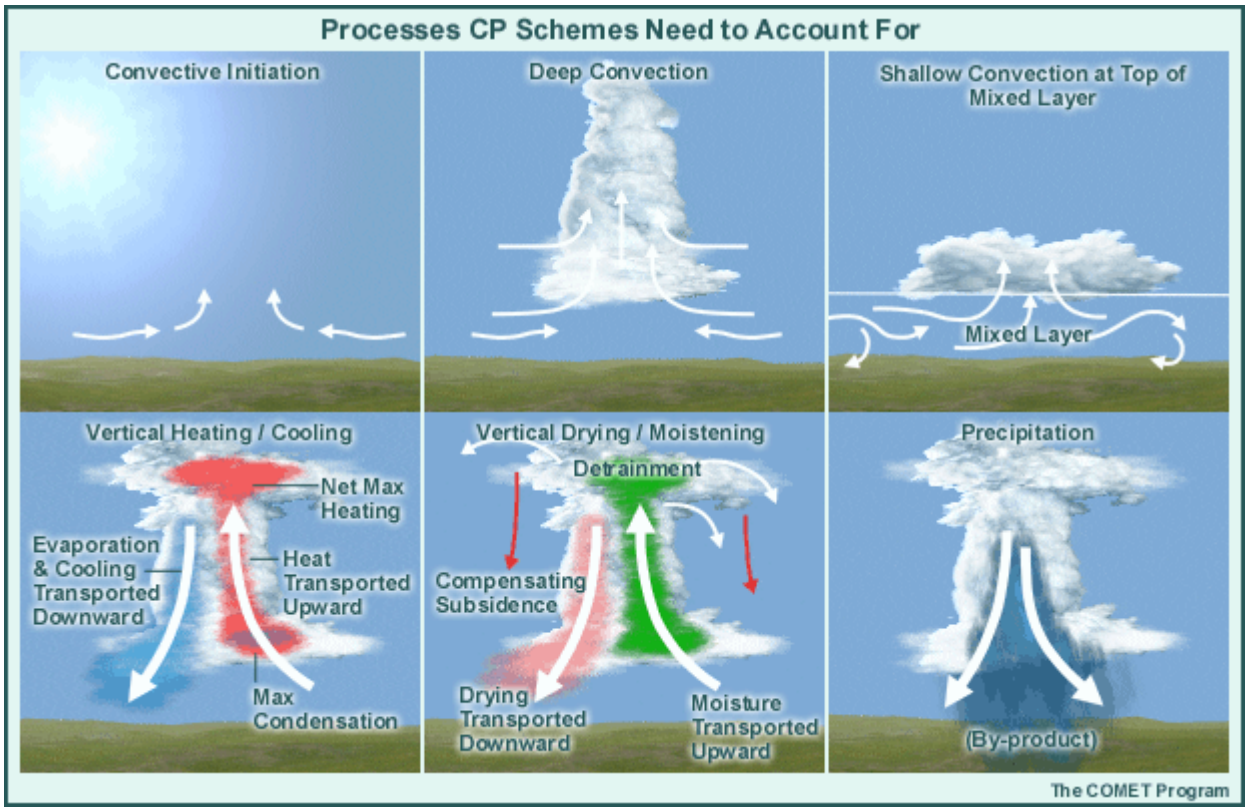

Figure 3.2 Processes which need to be included in GCM convection parametrizations. From: http://meted.ucar.edu/nwp/pcu1/ic3/frameset.htm

On the largest spatial scales and annual timescales these parameterisations have limited success. Figure 3.3 shows the zonal annual mean cloud cover as observed and as predicted by

an international selection of climate models. Most of the models reproduce the maxima in cloud observed in the tropics and in mid-latitudes but all underestimate the amount of cloud in the tropics and sub-tropics and overestimate it in mid- to high latitudes. For local cloud on timescales of hours, however, the predictions can be very poor.

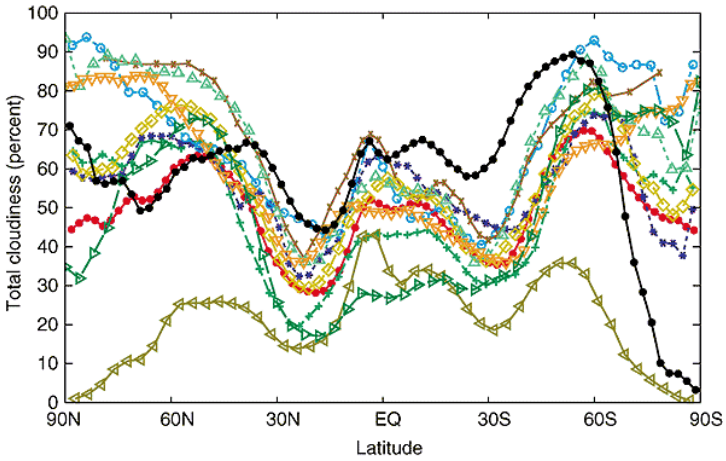

Figure 3.3 Zonal mean cloud cover from ISCCP data (in black) and as predicted by ten different global circulation models (coloured curves). From IPCC (2001).

Even disregarding the problems associated with predicting cloud distributions the models still need to calculate the effects of the cloud on the radiation fields. Again gross approximations have to be made in terms of the microphysical properties of the water or ice particles and the method by which to carry out necessary integrations over spectral and spatial variables (see section 4.2.4).

4. Radiative processes

Radiative processes are crucial in determining the climate of the Earth. Solar radiation is the fundamental energy source for the atmosphere while energy is lost from the globe by the emission of heat radiation. The circulations of the atmosphere and oceans essentially exist to transport solar energy from lower to higher latitudes. In this section we consider the Earth's Radiation Budget, review the mechanisms of radiative transfer within the atmosphere and discuss how these processes are treated within global climate models.

4.1. Earth Radiation Budget

The global average equilibrium temperature of the Earth is determined by a balance between the energy acquired by the absorption of incoming solar radiation and the energy lost to space by the emission of thermal infrared radiation. The amount of solar energy absorbed depends both on the incoming irradiance and on the Earth's reflective properties. If either of these changes then the temperature structure of the atmosphere-surface system tends to adjust to restore the equilibrium. In order to understand how these processes affect climate it is important to investigate in more detail the solar and infrared radiation streams. Figure 4.1 shows the components of the global annual average radiation budget and how much radiation is absorbed, scattered and emitted within the atmosphere and at the surface. The value for the incoming radiation, 342 W m^{-2}, is equivalent to a total solar irradiance at the Earth of 1368 W m^{-2} averaged over the globe. Of this 31 % (107 W m^{-2}) is reflected back to space by clouds, aerosols, atmospheric molecules and the surface, with the clouds playing the most important role, so that only 235 W m^{-2} is absorbed by the Earth system. 20 % (67 W m^{-2}) of the incident radiation is absorbed within the atmosphere leaving 49 % (168 W m^{-2}) to reach and heat the surface.

The temperature and emissivity of the surface are such that 390 W m^{-2} of infrared energy are emitted into the atmosphere. Only 40 W m^{-2} of this, however, escapes to space with the remainder being absorbed by atmospheric gases and cloud. The atmosphere returns 324 W m^{-2} to the surface. The energy balance at the surface is achieved by non-radiative processes such as evaporation and convection. The radiation balance at the top of the atmosphere is achieved by the 195 W m^{-2} of heat energy emitted to space by the atmosphere and clouds. The figure also gives an indication of how atmospheric and surface properties may affect the vertical temperature structure of the atmosphere. This is discussed further in section 4.2.2.

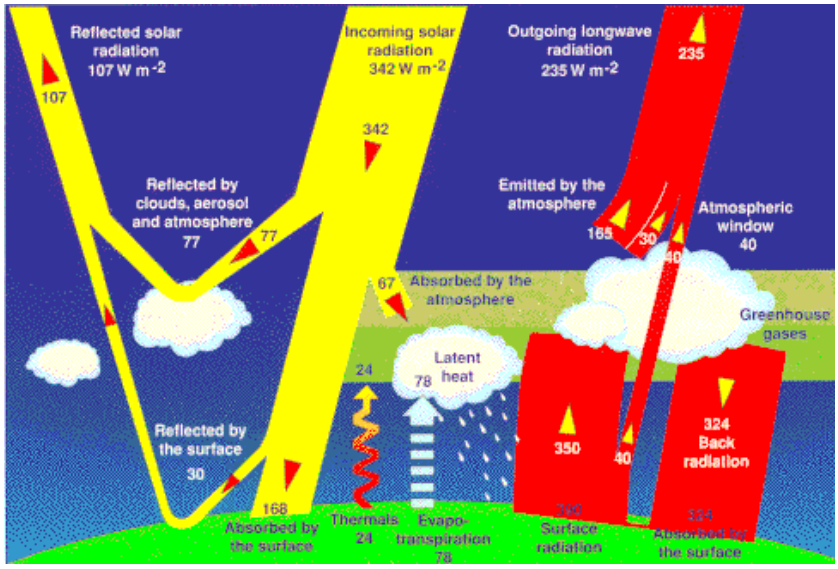

Figure 4.1 Globally averaged energy budget of the atmosphere. (Figure from http://asd-www.larc.nasa.gov/ceres/brochure/clouds-and-energy based on data from Kiehl and Trenberth, 1997).

The above picture considers only the global annual average situation. Hidden within this, however, are wide geographic and seasonal variations in the radiation budget components depending on incident solar radiation, surface reflectivity, cloud cover, atmospheric and surface temperatures and surface emissivity.

On a global annual average, if the climate is in an equilibrium state, the net top-of-atmosphere radiation fields are in balance. The concept of the radiative forcing of climate change, as used by the Intergovernmental Panel on Climate Change (IPCC 2001), is based on the empirical result that the equilibrium response in global average surface temperature is linearly related to a net imbalance imposed on the radiation budget. This imbalance might be brought about by, for example, an increase in greenhouse gas concentrations, tending to reduce outgoing longwave radiation and thus warm the climate, or an increase in surface albedo, tending to enhance the reflection of solar radiation and thus cool the climate. The coefficient of proportionality, referred to as the climate sensitivity parameter, has a value between 0.3 and 1.0 K W^{-1} m^2, depending on which climate model is used. The wide range is largely due to uncertainty in the feedback effects of changes in cloud amount (or properties) on the surface temperature. In the context of the effects of solar variability it is interesting to note that the increase in greenhouse gases since pre-industrial times (1750 say) gives a radiative forcing of about 2.4 W m^{-2}. To produce a similar effect (without any amplification factors) solar luminosity would have to increase by 1 %.

4.2. Radiative transfer

In order to simulate the radiation budget, and to calculate the radiative component of the diabatic heating term, Q, in equation (2.5), it is necessary to invoke the radiative transfer

equation. This gives the change in intensity $I_\lambda(s,\Omega)$ of radiation of wavelength λ in direction Ω between positions *s* and *s*+*ds* is as:

$$dI_\lambda(s,\Omega) = -\left\{I_\lambda(s,\Omega) - (1-\omega_\lambda)B_\lambda(s,\Omega) - \frac{\omega_\lambda}{4\pi}\int I_\lambda(s,\Omega')P_\lambda(s,\Omega,\Omega')d\Omega'\right\} k_\lambda \rho(s)ds \qquad (4.1)$$

where:

k_λ is the total extinction coefficient due to the absorption and scattering of radiation,

ω_λ is the single scattering albedo, i.e. the ratio of the scattering coefficient to the extinction coefficient,

$B_\lambda(s,\Omega)$ is the source function, i.e. the radiation emitted by the atmosphere (negligible at solar wavelengths but dominant in the thermal infrared) and

$P_\lambda(s,\Omega,\Omega')$ is the scattering phase function, i.e. the probability that radiation incident in solid angle Ω' will be scattered into Ω.

The first term on the right-hand-side of the equation represents removal (by absorption and scattering) of radiation from the incident beam, the second term represents emission into the beam and the third scattering into the beam of radiation incident from all other directions. The solution of this equation for radiation travelling upwards in a direction Ω_0 at altitude z_0 is:

$$I(z_t,\Omega_0) = I(0,\Omega_0)\mathrm{T}(0,z_0) + \int_0^{z_0}\left\{(1-\omega)B(z,\Omega_0) - \frac{\omega}{4\pi}\int_{4\pi} I(z,\Omega')P(z,\Omega',\Omega_0)d\Omega'\right\}\frac{d\mathrm{T}(z,z_0)}{dz}dz \qquad (4.2)$$

where the suffix λ has been dropped for simplicity but is still implied, $\mathrm{T}(z,z') = \exp(-\tau(z,z'))$ is the transmittance of the atmosphere (gases and clouds) between *z* and *z'* and the optical depth, τ, depends on the air density, ρ, the mass mixing ratio, *c*, the extinction coefficient, *k*, of the radiatively-active gas and the zenith angle, ζ, of the beam to the vertical according to: $\tau_\lambda(z) = \int_z^\infty k_\lambda c(z')\rho(z')\sec\zeta dz'$.

The first term on the right-hand-side of equation (4.2) represents radiation starting at the Earth's surface (either emitted or reflected) being transmitted to the height z_0. The second term integrates the transmission of radiation emitted and scattered by all atmospheric layers below z_0.

4.2.1. Absorption of solar radiation by the atmosphere

Absorption by the atmosphere of solar radiation depends on the concentrations and spectral properties of the atmospheric constituents. Figure 4.2 shows a blackbody spectrum at 5750 K, representing solar irradiance at the top of the atmosphere, and a spectrum of atmospheric absorption. Absorption features due to specific gases are clear with molecular oxygen and ozone being the major absorbers in the ultraviolet and visible regions and water vapour and carbon dioxide more important in the near-infrared.

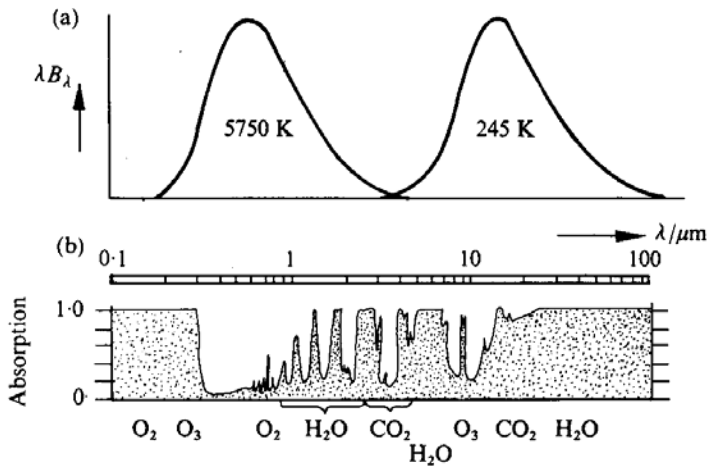

Figure 4.2(a) Black body functions at the emitting temperatures of the Sun and the Earth. The functions are scaled to have equal area to represent the Earth's radiation balance. (b) Absorption by a vertical column of atmosphere. The most important gases responsible for absorption are identified below, near the appropriate wavelengths. (Houghton, 1977)

The solar irradiance at any point depends on the properties and quantity of absorbing gases in the path above. The altitude at which most absorption takes place at each wavelength can be seen in Figure 4.3 which shows the altitude of unit optical depth for an overhead Sun. At wavelengths shorter than 100 nm most radiation is absorbed at altitudes between 100 and 200 km by atomic and molecular oxygen and nitrogen, mainly resulting in ionized products. Between about 80 and 120 km oxygen is photodissociated as it absorbs in the Schumann-Runge continuum between 130 and 175 nm. The Schumann-Runge bands, 175-200 nm, are associated with electronic plus vibrational transitions of the oxygen molecule and are most significant between 40 and 95 km altitude. The oxygen Herzberg continuum is found in the range 200-242 nm and is overlapped by the ozone Hartley-Huggins bands between 200 and 350 nm which are responsible for the photodissociation of ozone below 50 km. The ozone Chappuis bands, in the visible and near-infrared, are much weaker than the aforementioned bands but, because they absorb near the peak of the solar spectrum, the energy deposition into the atmosphere is significant. Furthermore, this deposition takes place in the lower atmosphere and so is particularly relevant for climate. The absorption of solar near-infrared by carbon dioxide and water vapour is smaller but makes an important contribution to the heat budget of the lower atmosphere (see section 4.2.2)

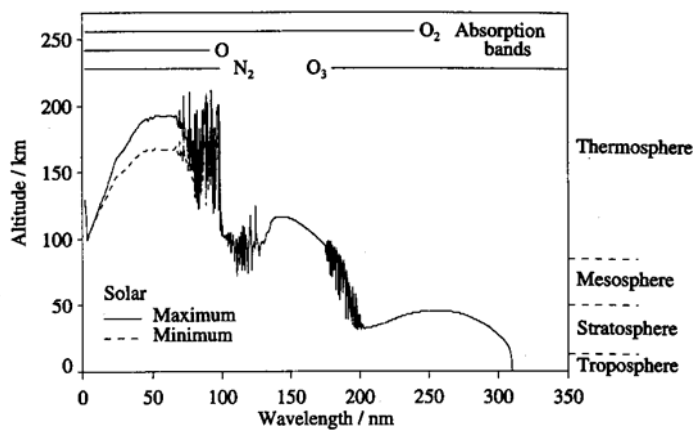

Figure 4.3 Wavelength dependence of the altitude of one optical depth for absorption of solar radiation with an overhead Sun. After Andrews (2000).

Solar irradiance varies with solar activity, as discussed in section 7.1, and the spectral composition of the variation determines which parts of the atmosphere respond most in terms of heating rates (see below). Note, however, that if the composition of the atmosphere were to

remain unchanged, then variations in irradiance do not affect the height of unit optical depth shown in Figure 4.3.

Most of the absorbed solar radiation eventually becomes heat energy so the local solar heating rate can be estimated from the divergence of the solar irradiance. Figure 4.4 shows the instantaneous heating rate spectrum as a function of altitude calculated for a tropical atmosphere with an overhead sun. Clearly visible are the strong absorption in the ultraviolet (wavenumbers > 25,000 cm^{-1}) in the upper stratosphere, in the visible (~14,000 – 25,000 cm^{-1}) throughout the stratosphere and in several narrow bands in the near infrared. Figure 4.5 presents a vertical profile of diurnally averaged solar heating rates for equatorial equinox conditions, showing the contribution of each of the UV/vis absorption bands mentioned below. This vertical structure in the absorption of solar radiation is crucial in determining the profile of atmospheric temperatures and plays an important role in atmospheric chemistry and thus composition.

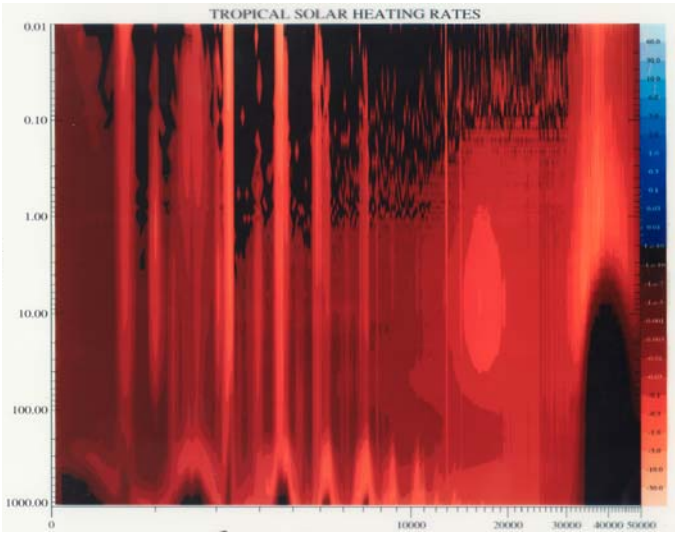

Figure 4.4 Solar heating rates as a function of wavenumber (=1/λ(cm)) and altitude (pressure in hPa), brighter red indicates greater heating. Figure courtesy of Gail Anderson.

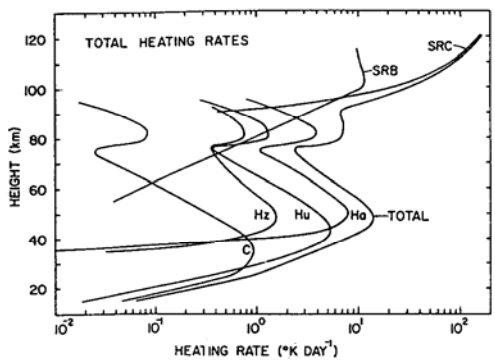

Figure 4.5 Diurnal average solar heating rate (K day^{-1}, log scale) as a function of altitude for equinoctial conditions at the equator showing contributions by the Schumann-Runge continuum and bands (SRC and SRB), the Herzberg continuum (Hz) and the Hartley (Ha), Huggins (Hu) and Chappuis (Ch) bands. After Strobel (1978).

If the solar spectral irradiance varies then, without a change composition, from the equation for the heating rate above we can see that the spectral heating rate just varies in proportion to the irradiance. If, however, as is actually the case, the atmospheric composition also responds to solar variability then this will affect both radiative fluxes and heating rates in a non-linear fashion. For example, an increase in incident solar radiation will tend to increase both but an increase in $c(z)$ (of ozone for example) will enhances τ tending to reduce the flux but increase the heating rate. The sign of the change at any altitude depends on the competition between these two factors which is determined by the spectral composition of the change in incident irradiance and its effects on the photochemistry of the atmosphere

4.2.2. Infrared radiative transfer and the atmospheric temperature structure

The atmosphere absorbs solar radiation, as discussed above, and, while this energy may at first be used in photodissociation, molecule excitation or ionization processes, it essentially ends up as molecular kinetic energy, i.e., in raising atmospheric temperatures. To balance this the atmosphere must lose heat by radiating energy in the thermal infrared. The amount of energy radiated depends on the local temperature and on the infrared spectral properties (emissivities) of the atmospheric constituents. Figure 4.2 shows a black body spectrum at 245

K, the radiative equilibrium temperature for a planet with albedo 31 % at approximately 1AU from the Sun, and the atmospheric absorption spectrum. Far infrared radiation is strongly absorbed by water vapour in its rotation bands and across the thermal infrared there are further water vapour absorption bands as well as features due to other "greenhouse" gases. There are strong carbon dioxide bands at 15μm, 4.3μm and 2.7μm, water vapour bands at 6.3μm and 2.7μm, an ozone band at 9.6μm as well as features due to methane, nitrous oxide and chlorofluorocarbons. Where the atmosphere is optically thin in the infrared, such as in the stratosphere, radiant heat energy may be transmitted to space, causing local cooling. At lower altitudes where the atmosphere is optically much thicker, however, emitted infrared radiation is absorbed and reemitted by neighbouring layers. Thus the atmospheric temperature profile is determined by interactions between levels as well as by solar heating and direct thermal emission.

In the middle atmosphere absorption of solar ultraviolet radiation by oxygen and ozone, as described in the previous section, produces a peak in temperature (the stratopause) near 50km. Above the ozone layer the effects of ultraviolet absorption by ozone are reduced and there is a minimum in temperature at the mesopause. Higher still, heating due to the absorption by molecular oxygen of far ultraviolet radiation takes over and there is a steep increase in temperature in the lower thermosphere.

The solar heating is counteracted by thermal emission, mainly by carbon dioxide in its 15 μm band, but also by the ozone 9.6 μm band and the water vapour 6.3 μm band. Typical profiles of infrared cooling and solar heating rates can be seen in Figure 4.6. The lower stratosphere (between approximately 15 and 25 km) is in approximate radiative equilibrium. Here heating is due to ozone absorption both of visible radiation in its Chappuis bands and also of infrared radiation emanating from lower levels in its 9.6 μm band. Cooling is mainly by carbon dioxide.

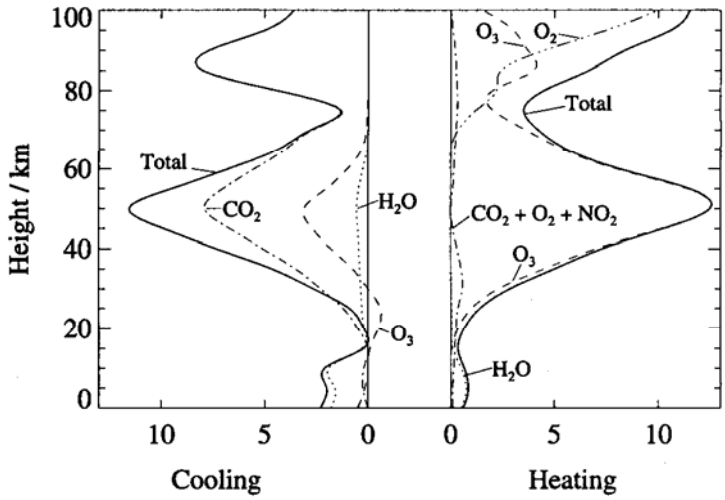

Figure 4.6 Global mean infrared cooling rates and solar heating rates (K d^{-1}) as a function of altitude showing contributions of the major gases. After Andrews (2000).

In the troposphere radiative transfer is largely accomplished by water vapour, and solar heating is relatively small. However, radiative processes do not determine the temperature profile in this region. This is because a radiative equilibrium profile would be convectively unstable, i.e., a small upward displacement of an air parcel would result in it remaining warmer than its environment, despite expansion and adiabatic cooling, and thus continuing to rise. The temperature profile of the troposphere is therefore limited by convective processes which result in the adiabatic lapse rate of about –7 K km^{-1}. Temperatures are locally warmer than would be the case based on radiative processes alone so that infrared emissions increase.

This results in infrared cooling due to tropospheric water vapour, as shown in Figure 4.6, rather than the warming which would come about from infrared trapping alone. Thus the tropopause marks the region where radiative processes (ozone heating and carbon dioxide cooling) take over from mainly convective processes. Note that an important factor determining the value for the temperature lapse rate is the release of latent heat from the condensation of water vapour into cloud droplets. Thus clouds play an integral part in determining the temperature structure of the lower atmosphere. The accurate representation of clouds and precipitation remains a major challenge in global climate modelling (see section 3.2).

4.2.3. Scattering of radiation

Scattering by cloud droplets and aerosols plays an important part in the redistribution of solar radiation and at thermal wavelengths scattering by ice cloud can also be significant. The scattering properties of clouds depend on their microphysical properties as well as their large scale structure. The former includes the phase, size, shape and density of the cloud particles as well as the wavelength of the radiation. Figure 4.7 shows that at visible wavelengths, except in the presence of very small drops, the reflection is almost independent of droplet size and depends only on optical depth. The near infrared reflectance, however, for thick clouds (optical depth $\tau > \sim 16$) depends not optical depth but only on particle size, with greater scattering for smaller drops. For thin clouds with small droplets the situation is more complex with no unique microphysical values for some pairs of spectral measurements.

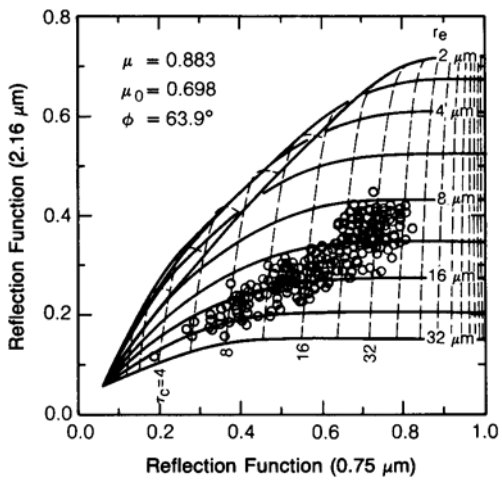

Figure 4.7 Curves: Theoretical relationship between the reflection at 0.75 and 2.16 µm of a cloud composed of spherical water drops as a function of optical depth (at 0.75 µm) and droplet radius. Solar zenith angle 45.7°, observation zenith angle 28°, relative azimuth 69°. Spots: measurements in stratocumulus cloud. Nakajima and King (1990).

For ice cloud the situation is even more complex because the ice crystals can not be assumed to be spherical. Figure 4.8 shows the phase scattering function (P in equation (4.1)) calculated for a spherical water droplet and for ice crystals with various shapes. All have a strong forward scattering peak but vary widely at different angles. The water droplet curve shows a rainbow feature at 140° and the hexagonal column curve the 23° halo often seen round the sun in the presence of thin cirrus cloud.

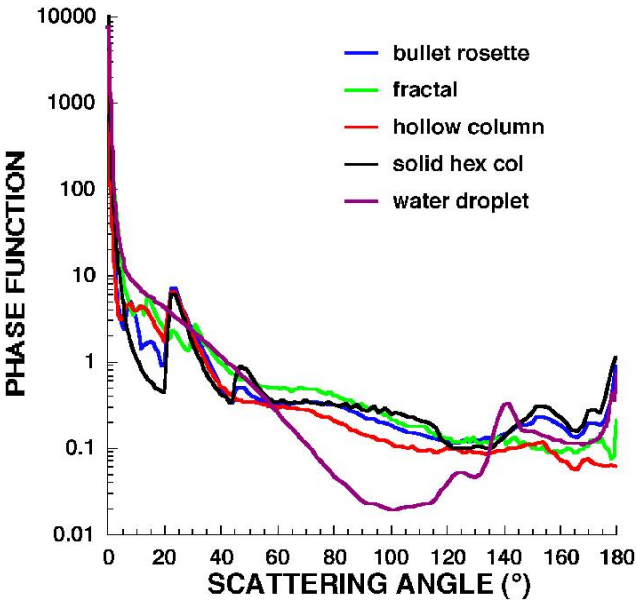

Figure 4.8 Phase scattering function for a spherical water droplet and for ice crystals of various shapes.

4.2.4. Drop size and optical depth

The scattering optical depth depends on the cross-sectional area of the droplets in the path of the radiation and can be expressed in terms of the droplet size distribution $n(r)$ by:

$$\tau \propto \iint r^2 n(r) dr dz$$

The liquid water path is the mass of water per unit area along the path of the radiation and so can be expressed as:

$$LWP \propto \iint r^3 n(r) dr dz$$

Thus we can relate τ to LWP by $\tau \propto \dfrac{LWP}{r_e}$

where the droplet effective radius is defined by $r_e = \dfrac{\int r^3 n(r) dr}{\int r^2 n(r) dr}$.

From this it becomes clear that if the total amount of liquid water available is fixed then the optical depth will be inversely related to droplet size. Thus if the number density of cloud condensation nuclei increases, the drop size will get smaller and the albedo of the cloud increase. This is the basis of the "indirect effect of aerosol" on radiative forcing and is also related to the link between cosmic rays and cloud discussed in section 7.4.

4.3. Radiation schemes in climate models

Equation (4.2) gives the expression for the intensity of monochromatic radiation travelling in a particular direction at a particular height in the atmosphere. Even to evaluate this one expression requires a large number of computations but to evaluate the diabatic source term (Q in equation 2.5) in a GCM it is necessary to integrate the expression over all angles and wavelengths. Clearly it is not computationally feasible to incorporate in a GCM the full details of the expression and a range of approximations need to be made. Some of these are listed, along with the associated reduction in a typical numbers of calculations, in Table 4.1. Each approximation brings a loss of accuracy and the choice of radiation scheme will be determined by a compromise between required accuracy and computational demands. The final row of the Table gives the Newtonian cooling approximation in which heating is assumed proportional to local temperature. This is usually not sufficiently accurate

(especially in the troposphere) and most GCMs adopt a band model approach. The number of spectral bands necessary also depends on the height regime of the model. For example, if it is intended to assess the effects of solar UV radiation in the middle atmosphere then extra shortwave bands need to be added to GCM radiation schemes which have been designed for use in the troposphere.

Table 4.1 Approximations in the radiative transfer equation (neglecting scattering) and the number of calculations needed for each component integral. Note that the total number is the product, not the sum, of the components because the integrals are nested. The final column gives the number of exponential functions that need to be estimated – each adding a further computational overhead.

Approximation	Sum over spectral lines in expression for optical depth	Integration over height in expression for optical depth	Integration over height of irradiance contributions	Integration over zenith angle	Integration over wavelength	Total number of calculations	Number of exponentials in transmittance and Planck functions
None	1-10	10-100	10-100	1-10	10^4	$10^6 – 10^{10}$	10^5-10^6
Curtis-Godson	1-10	-	10-100	1-10	10^4	$10^5 – 10^8$	10^5-10^6
Diffusivity	1-10	-	10-100	-	10^4	$10^5 – 10^7$	10^5-10^6
Band model	-	-	10-100	-	1-10	$10 – 10^3$	$10 – 10^3$
Newtonian cooling	-	-	-	-	-	1	-

Note that Q needs to be estimated, as a function of model state, at each gridpoint and on most timesteps so that, even using the band model approximation, about 40% of a GCM's demands on CPU time will be accounted for by the radiation scheme.

5. Photochemistry

The interaction of solar radiation with the atmosphere is key to the initiation of many of the chemical processes which take place. Here we consider the role of solar UV radiation in determining the budget of stratospheric ozone. In section 7 we will discuss how the composition and thermodynamic structure of the stratosphere are modulated by solar variability and also how radiative perturbations to the upper stratosphere may impact winter polar dynamics.

5.1. Stratosphere

In the stratosphere the main chemical reactions determining the concentration of ozone are:

$$O_2 + h\nu \rightarrow O + O$$

$$O + O_2 + M \rightarrow O_3 + M$$

$$O_3 + h\nu \rightarrow O_2 + O$$

$$O + O_3 \rightarrow 2O_2$$

$$O_3 + X \rightarrow XO + O_2$$

$$XO + O \rightarrow X + O_2$$

The first of these reactions represents the photodissociation of oxygen at wavelengths less than 242 nm. This process is the key step in ozone formation because the oxygen atoms produced react with oxygen molecules to produce ozone molecules, as depicted in the second reaction (the M represents any other air molecule whose presence is necessary to simultaneously conserve momentum and kinetic energy in the combination reaction). Because the short wavelength ultraviolet radiation gets used up as it passes through the atmosphere, concentrations of atomic oxygen increase with height. This would tend to produce a similar

profile for ozone but the effect is counterbalanced by the need for a 3-body collision (reaction 2) which is more likely at higher pressures (lower altitudes). Thus a peak in ozone production occurs at around 50 km. The third reaction is the photodissociation of ozone, mainly by radiation in the Hartley band ($\lambda < 310$ nm), into one atom and one molecule of oxygen. This does not represent the fundamental destruction of the ozone because the oxygen atom produced can quickly recombine with an oxygen molecule. The fourth reaction represents the destruction of ozone by combination with an oxygen atom. The fifth and sixth reactions represent the destruction by any catalyst *X*, which may include *OH*, *NO* and *Cl*. The various destruction paths are important at different altitudes but the combined effect is an ozone concentration profile which peaks near 25 km in equatorial regions.

Because photodissociation is an essential component of ozone formation most ozone is produced at low latitudes in the upper stratosphere. Observations show, however, that it is also present in considerable quantities in the mid- and high latitude stratosphere due to transport by the mean meridional circulation (see section 1.3). The resulting distribution of mixing ratio is shown in Figure 5.1. The atmospheric circulations tend to move the ozone away from its source region towards the winter pole and downwards. Indeed, the quantity of ozone above unit area of the Earth's surface (referred to as the ozone column amount) is usually greater at mid-latitudes than the equator, see In the lower stratosphere its photochemical lifetime is much longer, because of the reduced penetration of the radiation which destroys it, and its distribution is determined by transport, rather than photochemical, processes. In winter high latitudes photochemical destruction essentially ceases and the ozone accumulates until the spring.

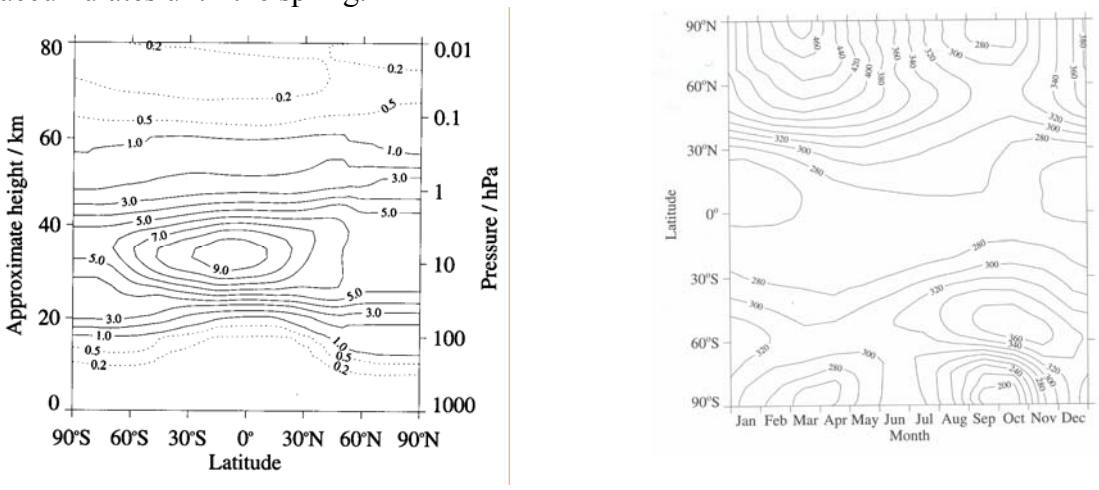

Figure 5.1 Left: Zonal mean concentration of ozone (ppmv) in January. Right: The annual cycle in the latitudinal distribution of zonal mean ozone column amounts. The units are 10^{-3} atm cm (1 atm cm = 2.69 x 10^{19} molecules cm^{-2}). From: Andrews (2000).

The minimum in ozone column which occurs near the south pole in spring (October) has deepened considerably during the past thirty years into what has become known as the "ozone hole". Observations and theoretical studies have shown that the depletion occurs mainly in the lower stratosphere and is due to catalytic destruction of ozone on the surface of polar stratospheric cloud particles by active chlorine which is released as the sun rises in spring from chlorine compounds which have been stored through the winter. The source of the chlorine is CFCs which are now banned under international agreement. Because of the long atmospheric lifetime of CFCs and the natural interannual variability of the winter polar atmosphere it is difficult to see a trend over short (few year) periods but it appears that the ozone hole is now filling.

5.2. Troposphere

Solar radiation is also fundamental in determining the composition of the troposphere. The daytime chemistry of the troposphere is dominated by the hydroxyl radical, OH, because its high reactivity leads to the oxidation and chemical conversion of most other trace constituents. OH is formed when an excited oxygen atom, $O(^1D)$, reacts with water vapour. The source of the $O(^1D)$ is the photodissociation (at wavelengths less than about 310 nm) of ozone; thus the presence of ozone is fundamental to the system. A major source of tropospheric ozone is transport from the stratosphere, but it is also formed through the photolysis (at wavelengths less than 400 nm) of nitrogen dioxide, which can be catalytically regenerated. Because OH is photolytically produced its concentration drops at night and the dominant oxidant becomes the nitrate radical, NO_3, itself photochemically destroyed during the day.

Thus any variation in the intensity, or spectral composition, of solar radiation may affect the lower atmosphere not only through direct heating but also potentially through modifying its chemical composition.

6. Modes of variability in the atmosphere

6.1. Modes of variability

The atmosphere exhibits a number of characteristic modes of variability that are important in determining the local climate in various regions. A discussion of the physical bases of these modes is beyond the scope of this course but descriptions of some of them are included as they may influence how the impact of solar variability on climate is experienced.

Identified modes of variability are several, each with different geographical influences, but all showing specific patterns of response with large regional variations. The El Niño-Southern Oscillation (ENSO) phenomenon is the leading mode in the tropics, although its influence is felt globally. At higher latitudes the leading northern winter modes are the North Atlantic Oscillation (NAO) and the Pacific-North America Oscillation (PNA), which are sometimes viewed as part of the same phenomenon, referred to as the Arctic Oscillation (AO) or Northaern Annular Mode (NAM). There is an Antarctic Oscillation (AAO), or Southern Annular Mode (SAM), in the southern hemisphere. In the equatorial lower stratosphere a Quasi-Biennial Oscillation (QBO) modulates winds and temperatures.

It has been suggested that the impact of solar variability, as well as other climate forcing factors, may be to affect the frequency of occupation of certain phases of these modes. Below follows some short descriptions of the modes. In section 7.5 will be discussed how they have been proposed to respond to solar activity.

6.1.1. The North Atlantic Oscillation

Over the Atlantic in winter the average sea level pressure near 25-45°N is higher than that around 50-70°N. This pressure gradient is associated with the storm-tracks which cross the ocean and determine, to a large extent, the weather and climate of western Europe. Since the 1930s it has been known that variations in the pressure difference are indicative of a large-scale pattern of surface pressure and temperature anomalies from eastern North America to Europe. If the pressure difference is enhanced then stronger than average westerly winds occur across the Atlantic, cold winters are experienced over the north-west Atlantic and warm winters over Europe, Siberia and East Asia, with wetter than average conditions in Scandinavia and drier in the Mediterranean. The fluctuation of this pattern is referred to as the

NAO and the pressure difference between, say, Portugal and Iceland can be used as an index of its strength, see Figure 2.1. Some authors regard the NAO as part of a zonally symmetric mode of variability, the AO, characterized by a barometric seesaw between the north polar region and mid-latitudes in both the Atlantic and Pacific.

Using individual station observational records of pressure, temperature and precipitation, values for the NAO index have been reconstructed back to the seventeenth century. The index shows large inter-annual variability but until recently has fluctuated between positive and negative phases with a period of approximately four or five years, see Figure 6.1. Over the past two decades the NAO has been strongly biased towards its positive, westerly, phase and it has been suggested that this might be a response to global warming.

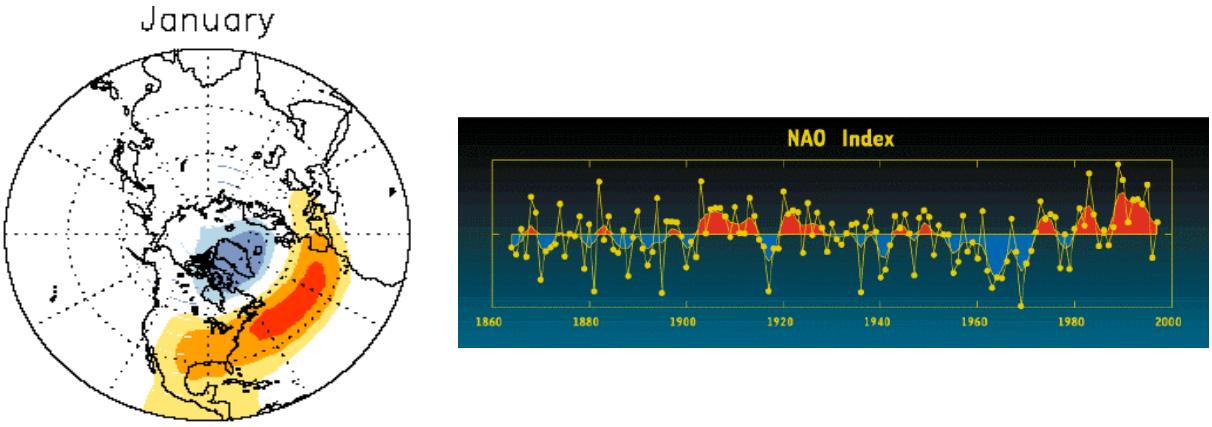

Figure 6.1 Left: Pattern of anomalies in surface pressure for the positive phase of the NAO (red=+ve, blue=-ve). Right: time series of NAO index. From: http://www.ldeo.columbia.edu/res/pi/NAO/

Another uncertainty is how significant might be coupling with either sea surface temperatures and/or the state of the middle atmosphere in producing a realistic NAO/AO pattern. Planetary-scale waves, produced in the lower atmosphere by longitudinal variations in topography, propagate upwards in winter high latitudes through the stratosphere and deposit momentum and heat which feeds into the general atmospheric circulation. Where this wave absorption takes place depends on the ambient temperature and wind structure. Thus any changes induced in the mean temperature structure of the stratosphere may result in a feedback effect on lower atmosphere climate. An analysis of zonal wind observations does suggest a downward propagation of AO patterns in many winters (Baldwin and Dunkerton, 2001). This offers a plausible mechanism for the production of NAO/AO-type signals in tropospheric climate by factors which affect the heat balance of the stratosphere (Kodera, 1995), specifically solar variability. Data and modelling studies have already shown such a response to heating in the lower stratosphere by volcanic eruptions (Robock, 2001).

6.1.2. The El Niño-Southern Oscillation

The El Niño was the name given to the periodic warming of the ocean waters near the coast of Peru and Ecuador which adversely impacts the fishing industry in this region due to the suppression of upwelling nutrient-rich deep waters. The Southern Oscillation was the term used to describe a periodic variation observed in the east-west gradient of surface atmospheric pressure across the equatorial Pacific. It is now realised that these two phenomena are both parts of the same complex interaction of the ocean and atmosphere, subsequently referred to as ENSO. In an ENSO event positive anomalies of sea surface temperature initially appear on

the east side of the equatorial Pacific and over a period of a few months spread westward until they cover most of the ocean at low latitudes, as shown in Figure 6.2.

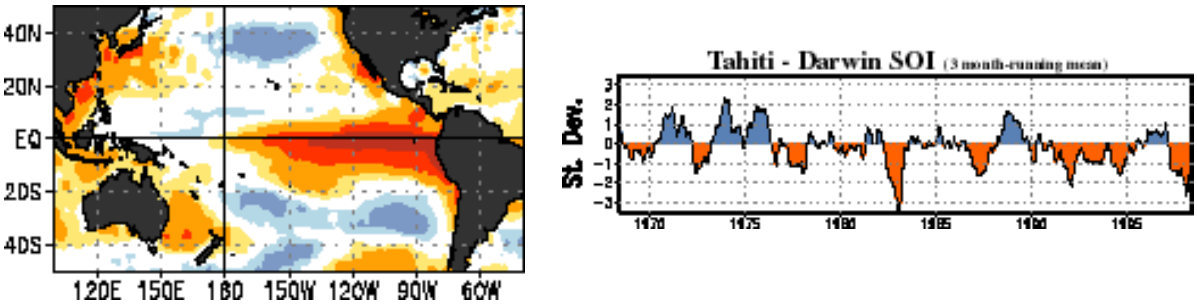

Figure 6.2 Left: Anomalies in Pacific sea surface temperatures associated with ENSO. Right: time series of ENSO index. From: http://www.cpc.ncep.noaa.gov/products/analysis_monitoring/ensocycle /enso_cycle.html

Associated with this the region of maximum rainfall, normally over the maritime continent, shifts eastward into the Pacific. A wide range of interannual climate anomalies, in the extra-tropics as well as near the equator, appear to be associated with ENSO but there is not, as yet, a complete theory which can explain the complex coupling of the atmospheric and oceanic dynamics and thermodynamics which is taking place. ENSO events occur every 2-5 years but seem to have been increasing in frequency over the past two decades, see Figure 6.2.

6.1.3. The Quasi-Biennial Oscillation

In the equatorial lower stratosphere an oscillation in zonal winds occurs with a period of approximately 28 months. A given phase (east or west) starts in the upper stratosphere and moves downward at a rate of about 1km per month to be replaced by winds of the opposite phase (see Figure 6.3). The largest amplitude in the zonal wind variation occurs at about 27 km altitude. The QBO comes about because of interactions between vertically propagating waves and the mean flow. When the wind blows from the west (QBO west phase) westward moving waves can propagate freely but eastward moving waves are absorbed and deposit their momentum, thus strengthening the existing westerlies and moving the westerly peak downwards. Somewhat above this absorption layer the westward moving waves are dissipated and weaken the west wind, eventually changing the direction to easterly. The absorption of the westward waves then starts to propagate downwards, reversing the phase of the QBO. Baldwin et al. (2001) give a good review of current understanding of the QBO.

The effects of the QBO are not restricted to equatorial regions. The transport of heat, momentum and ozone to high latitudes are all modulated. On average the westerly phase of the QBO is associated with colder winter temperatures at the north pole in the lower stratosphere. This can be explained by an enhanced ability of mid-latitude planetary waves to propagate into the equatorial westerlies leaving the cold winter pole undisturbed. However, this relationship only appears to hold when the Sun is at lower levels of activity. Near 11-year cycle maxima the relationship breaks down and possibly reverses. The absorption of solar radiation is greater in the stratosphere than lower down and its modulation by solar activity quite significantly larger. The potential for solar modulation of stratospheric temperatures and winds to modify planetary wave propagation, and hence tropospheric climate, is an active area of research.

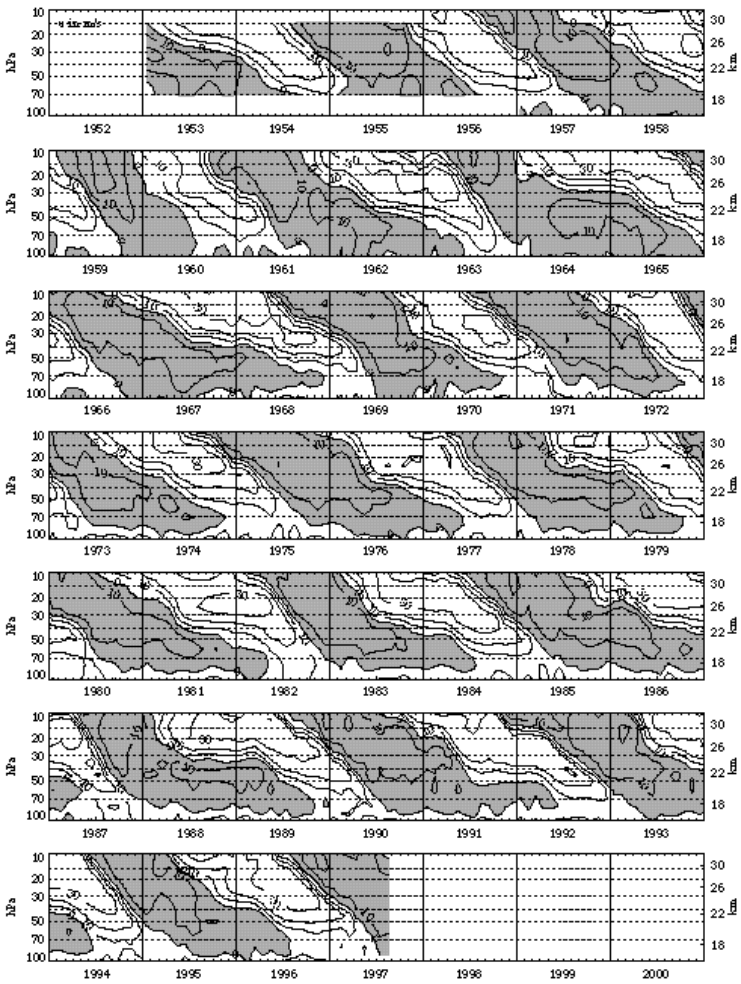

Figure 6.3 A time series of the zonal wind profile above Singapore. The downward propagation of alternating easterly and westerly winds is the QBO.

Signals with a periodicity of 2-3 years have also been found in records of surface temperature and precipitation and, recently, in the NAO index. This interaction between modes presents a much more complex picture but again suggests a mechanism whereby the response of climate parameters to solar variability could have a marked geographical distribution.

6.2. Representation in climate models

Computer models of the general circulation of the atmosphere are quite successful in simulating NAO-type variability and it appears as a leading mode in many climate models, even those without a coupled ocean. Furthermore, some GCM studies show increasing values of the NAO index when concentrations of greenhouse gases are enhanced (Shindell et al, 1999a). However, this is not true of all models' results and some studies suggest that the NAO pattern itself may be modified in a changing climate so that use of simple indices may not be appropriate.

Coupled atmosphere-ocean models show sea surface temperature variability in the tropical Pacific which has some similarity to ENSO. However, they tend to show too weak interannual variability in the eastern equatorial Pacific and too strong in the central equatorial Pacific (Latif et al, 1999). To improve this some models are now adopting an enhanced horizontal resolution in the tropics to better resolve ocean dynamics. State-of-the-art models show some success in the (seasonal) prediction of El Niño events although the timing and strength of the predictions are sensitive to details of the initial state. The implementation of

ocean data assimilation, together with higher resolution and improvements in model physics, is anticipated to improve the El Niño predictions.

Traditional climate models show no indication of QBO-type behaviour and, until recently, neither did models extending through the middle atmosphere. However, two factors have emerged as important in facilitating its simulation. The first is a better representation of vertically-propagating gravity waves; these are buoyancy waves that are generally of too small wavelength to be explicitly resolved by climate models but whose effects on the momentum budget of the middle atmosphere, particularly the mesopause region, are known to be significant. Improved gravity wave schemes, which are able to simulate the propagation of a spectrum of waves through, and interaction with, the stratosphere have now been implemented (e.g. Warner and McIntyre, 2001). The other factor is the model's vertical resolution an increase in which has been shown to produce QBO-type variability in the tropical lower stratosphere (Butchart et al, 2003). However, the period of the oscillation, and the downward propagation speed of the wind anomalies, is highly sensitive to tuneable parameters in the model schemes so it is likely that some interactions are not being fully represented.

7. Solar variability and climate modelling

The discussion above has focussed on the techniques used in GCMs to represent atmospheric processes. Here we consider the ways in which solar variability may induce climate change and to what extent these are currently represented in climate models.

7.1. Radiative heating

Total solar irradiance varies with solar activity, as presented in WP101. A simple approach to assessing the effects of this on global average temperature is to use an energy balance model. An example of some EBM estimates of the evolution of global average surface temperature over the past 1000 years in response to various forcing factors is given in Figure 7.1. The upper panel shows the separate responses to changes in greenhouse gases, tropospheric aerosol, stratospheric (volcanic) aerosol and three different TSI series. The lower panel shows the response estimated to a combination of forcing factors, along with observational and reconstructed measurements of surface temperature.

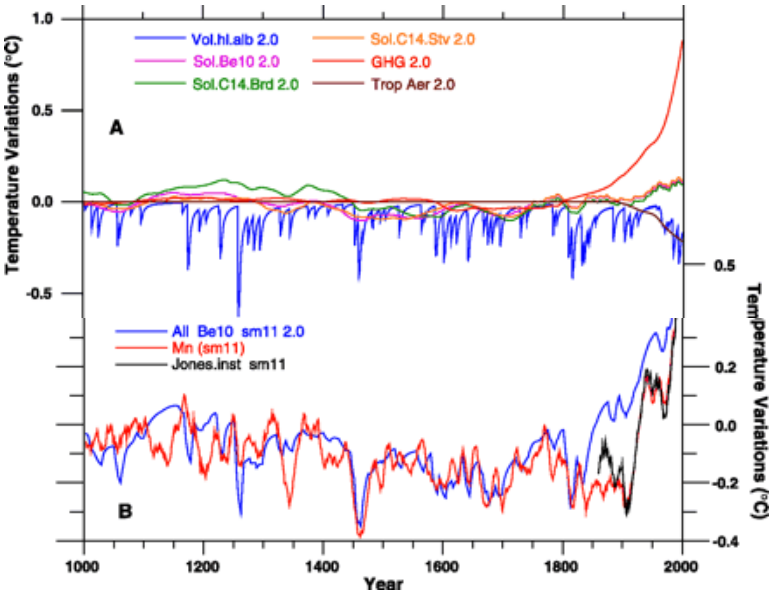

Figure 7.1 Global average surface temperature calculated using an EBM. Top: results for individual forcings. Bottom: result for combined forcings (in blue) compared with the observational record (in black) and a series reconstructed from proxy data (red). (Crowley, 2000)

The results suggest that the gross features of the temperature record are determined by volcanic and solar drivers until the twentieth century when human-induced factors, especially greenhouse gases, dominate.

Figure 7.2 shows estimates of global mean surface temperature calculated for the past 150 years using a full GCM. These results show that quite a good match between modelled and observed values can be obtained by including both natural (solar and volcanic) as well as anthropogenic forcings with the increase in solar irradiance being particularly important in producing the warming over the first half of the twentieth century.

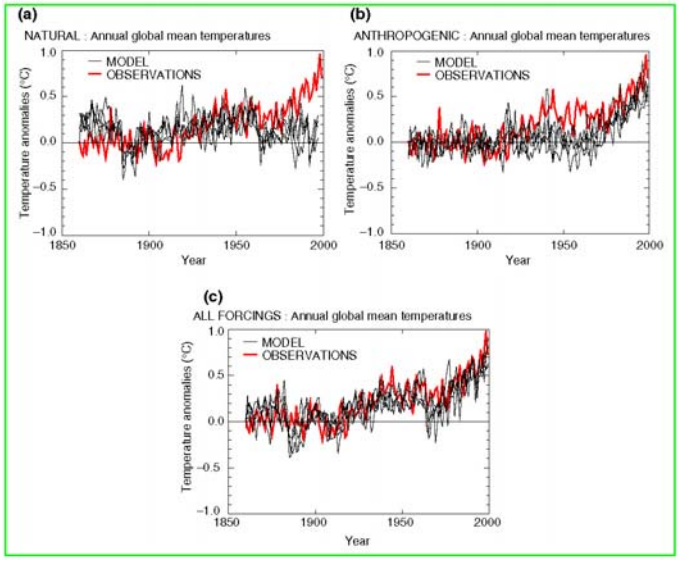

Figure 7.2 Global annual mean surface temperature calculated using a GCM. Each panel shows 4 model integrations with the same forcing, giving an indication in intrinsic natural variability. (IPCC, 2001)

However, there is a large amount of noise in both the model and the observational datasets. An alternative approach to detecting component causes of climate change, is "optimal fingerprinting". Here it is assumed that the geographical patterns of response to particular factors are known, that the time-dependences of the forcing factors are known but that the amplitudes of the responses are unknown. The task is then essentially to perform a multiple regression analysis on a dataset to find which weighted combination of the response patterns best matches the data, taking into account known errors/uncertainties in both the data and patterns. An example of the results of one such analysis, using a dataset of surface temperature observations on a latitude-longitude grid over the twentieth century, is shown as global averages in Figure 7.3(a). The black curve is the observations with the grey band representing measurement uncertainty; the red curve shows the result of only using anthropogenic forcing factors, the green only natural factors and the blue both together. A good fit is obtained when both types of forcing are included but Figure 7.3(b) shows the derived magnitudes of the forcings. Here the value 1 indicated that the derived magnitude equals that the model gives using standard radiative forcing estimates. The model appears to be underestimating the solar influence by a factor of 2 or 3 implying that some amplification factors of the solar influence are not incorporated into the model's representation (Stott et al 2003).

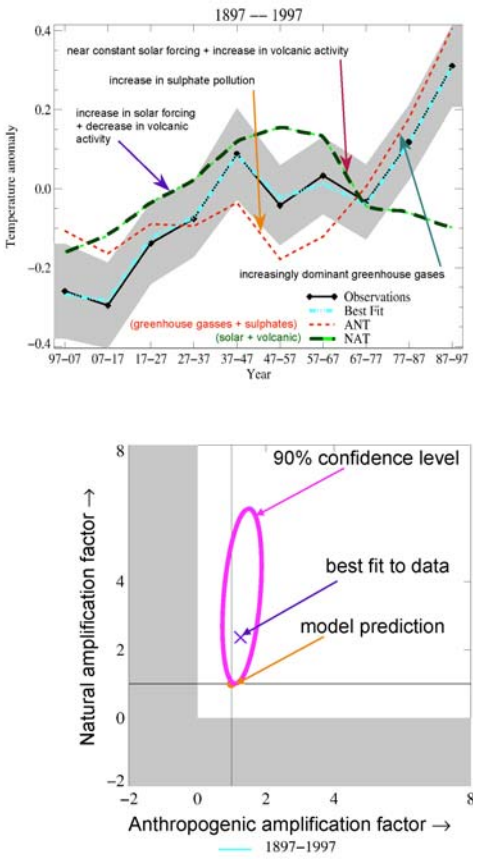

Figure 7.3 Optimal fingerprinting technique in which geographical patterns of surface temperature change for different forcings are fitted to the observed time series. Top: results for different forcing factors, Bottom: derived magnitude of natural and anthropogenic forcings relative to that found from standard model runs.

Furthermore, GCM runs which only include variations in TSI are unable to reproduce the distributions of the response of temperature and geopotential height shown in WP103. To explain these underestimates it is necessary to find some factor(s) which amplify the effect from that derived simply by consideration of total solar irradiance as the primary driving mechanism behind the impact of solar variability on climate.

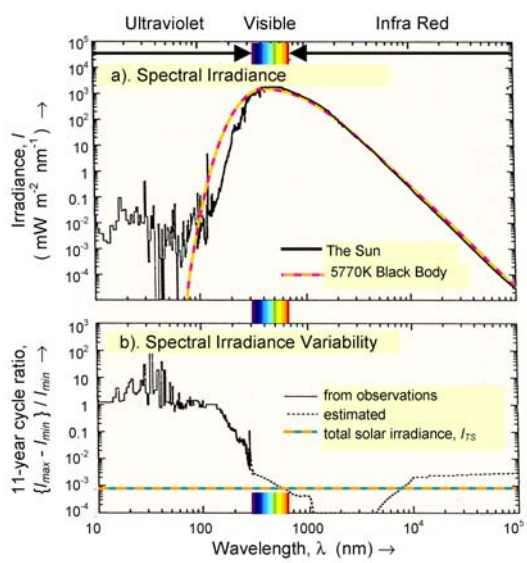

Figure 7.4 Top: solar spectrum. Bottom: Fractional difference in solar spectral irradiance between maximum and minimum of the 11-year cycle. Adapted from Lean (1991) by M. Lockwood.

Potentially one such amplification mechanism is through the effects of variations in solar UV radiation on the stratosphere. Over the solar cycle total solar irradiance varies by about 0.1% but in the UV variations are much larger (see Figure 7.4). These shorter wavelengths are

absorbed in the stratosphere and above so it is at these higher altitudes that the largest effects on temperatures will be felt. Note that only models in which the radiation scheme has sufficient spectral resolution will the height structure of the heating rate impact be correctly simulated.

7.2. Temperatures

The response of atmospheric temperatures to solar variability is large in the upper atmosphere, with thermospheric variations of order 100 K being typical over the 11-year cycle, reflecting the large modulation of far ultraviolet radiation in that region. At lower altitudes the response is smaller, and less certain. Measurements made from satellites suggest an increase of up to about 1 K in the upper stratosphere at solar maximum, a minimum, or even negative, change in the mid-low stratosphere with another maximum, of a few tenths of a degree below. However, precise values, as well as the position (or existence) of the negative layer, vary between datasets: some examples are given in Figure 7.5.

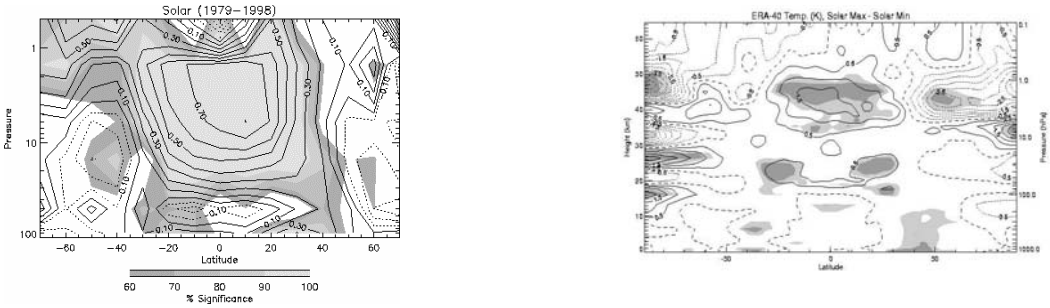

Figure 7.5 Difference in temperature between solar maximum and solar minimum derived from observational data. Left: SSU/MSU satellite data (grey shading denotes statistical significance as shown in the legend). Right: ERA reanalysis data for the period 1979-2001; light/dark shading denotes 95% and 99% significance. Note the different height ranges in the two panels. (SOLICE, 2004)

Studies of the solar influence using middle atmosphere GCMs also show a range of responses. Figure 7.6 Presents the temperature change predicted by five different GCMs with three different approaches to implementing the necessary change in ozone. The best agreement is shown between the ERA data and the GCM with coupled chemistry but there remain large uncertainties in the nature of the response.

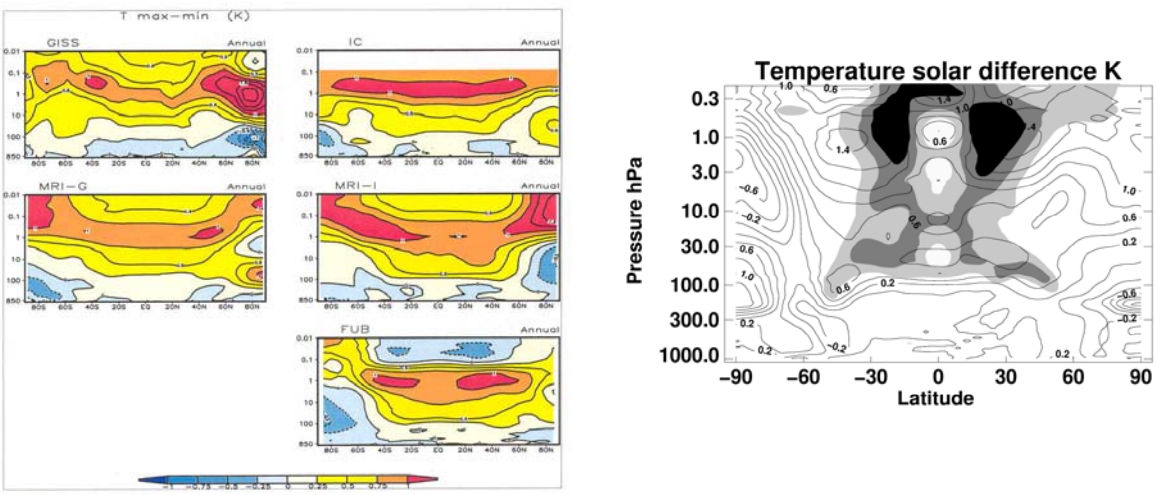

Figure 7.6 Results from GCM simulations of the response of middle atmospheric temperatures to the 11-year solar cycle. The first column shows runs of two different GCMs which have both specified a solar-induced ozone response. The second column contains similar experiments but with a different specified

ozone field (SOLICE, 2004). The panel in the third column comes from a GCM with a coupled chemistry scheme and thus an interactively-produced ozone response.

During the winter the high latitude stratosphere becomes very cold and a polar vortex of strong westerly winds is established. The date in spring when this vortex finally breaks down is very variable, particularly in the northern hemisphere, but plays a key role in the global circulation of the middle atmosphere. In a series of studies Kuni Kodera has suggested that, because variations in solar UV input change the latitudinal temperature gradient in the upper stratosphere, the evolution of the winter polar vortex will be affected. The first column in Figure 7.7, derived from satellite data, shows that the vortex strengthens in November and December in response to solar activity and this positive anomaly in zonal mean zonal winds then propagated polewards and downwards until by February it is replaced by an easterly anomaly.

The other columns in Figure 7.7 Show the results of various GCM runs. None is successful in reproducing the apparent observational signal. It remains to be seen whether this disparity is due to fundamental flaws in the models, or to the design of the experiments, to insufficiently long integrations or even lack of statistical significance in the observational data analysis.

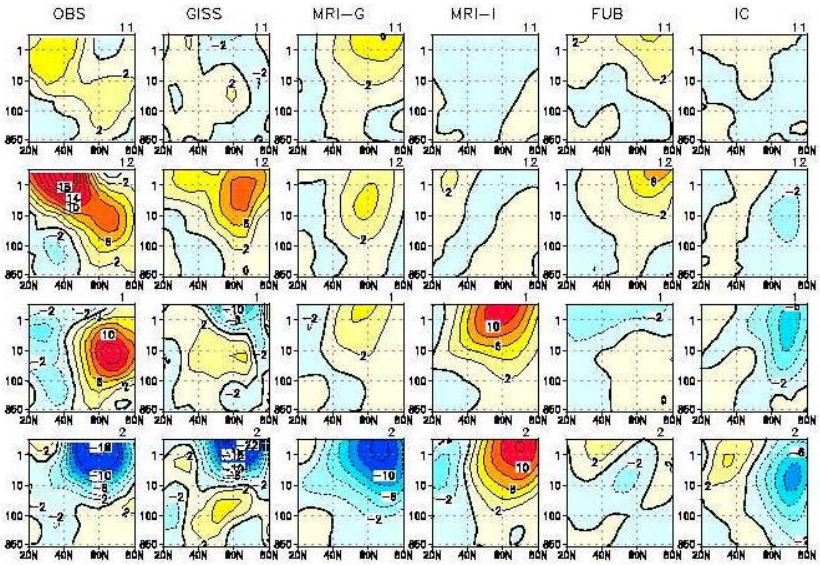

Figure 7.7 Difference between solar maximum and solar minimum in Northern Hemisphere zonal mean zonal wind from November (top) to February (bottom). First column from satellite measurements; other columns different GCMs (Matthes et al, 2003).

The first GCM studies of the impact of solar UV-induced variations in stratospheric temperature and ozone (see below) on the dynamical structure of the troposphere were presented by Haigh (1996). In that paper a number of experiments were carried out using a variety of assumptions concerning ozone changes. All the experiments showed the same pattern of response in tropospheric temperatures and winds but with different magnitudes depending on the specifications of the UV and ozone changes. At higher solar activity the sub-tropical jets are shown to be weaker and move slightly poleward. This theoretical result is similar to that determined to be the solar signal in observational data, though somewhat weaker in amplitude (see Figure 7.8). This work is beginning to provide an understanding of how, through the spectral composition of solar irradiance, apparently small changes in TSI may significantly impact the circulation of the lower atmosphere. More work is needed, however, to establish details of the mechanisms whereby these effects take place.

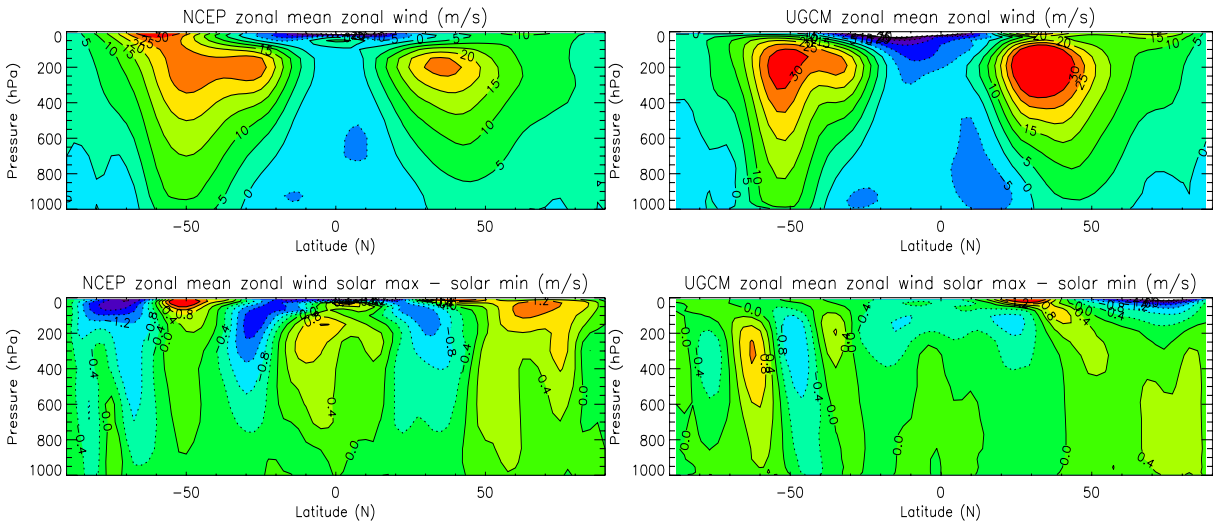

Figure 7.8 Left: Top: annual average zonal mean westerly wind from NCEP data; bottom: difference between solar max and solar min from a multiple regression analysis of the NCEP data (Haigh et al 2005). Right: the same but from a model simulation in which solar UV radiation and stratospheric ozone have been changed to represent solar cycle variability (Haigh, 1999).

7.3. Photochemistry

Another factor is important in determining the stratospheric response is the effect of enhanced UV on ozone. According to the photochemistry outlined in section 5.1 the ozone production, at shorter wavelengths, will be more strongly modulated by solar variability than its destruction and thus there is a higher net production of ozone when the sun is more active.

Both observational records and model calculations show approximately 2 % higher values in ozone columns at 11-year cycle maximum relative to minimum. However, there are some discrepancies between satellite observations and model predictions in the vertical and latitudinal distributions of the response. Equatorial profiles of ozone solar cycle modulation from a selection of model calculations and two satellite data analyses, are shown in Figure 7.9. The models all show the same shape profile shape while the observational datasets suggest something rather different: a larger response near the stratopause and possibly a second maximum in the lower stratosphere.

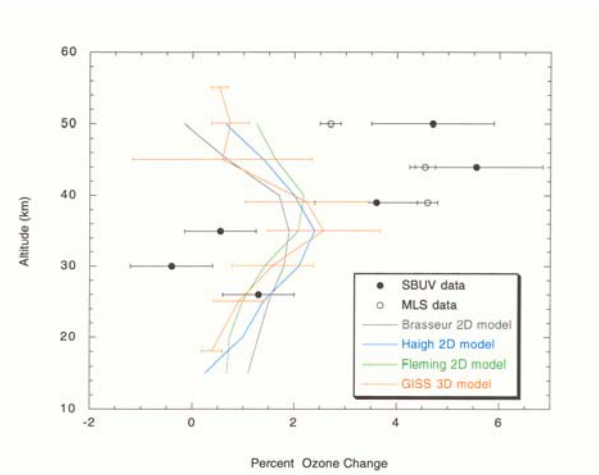

Figure 7.9 Estimates of percentage increase in tropical ozone from solar min to solar max from satellite data (data points and horizontal bars) and models (coloured curves). Shindell (1999b)
.

Figure 7.10 (lower panel) shows a typical model calculation with largest changes in the middle stratosphere and less above and below while the upper panel shows the solar cycle

modulation of ozone derived from the SAGE satellite dataset. This remains a key area of uncertainty in solar effects on the atmosphere. There may be some factors missing in the models and their poor simulation of the lower stratospheric response suggests this might be related to ozone transport. However, full 3D GCMs produce very similar profiles to those of the 2D models with less complete dynamics so the mechanisms involved are not clear. It should also be borne in mind that the observational data are only available over less than two solar cycles so there remains some doubt about the statistical robustness of the signals derived from them.

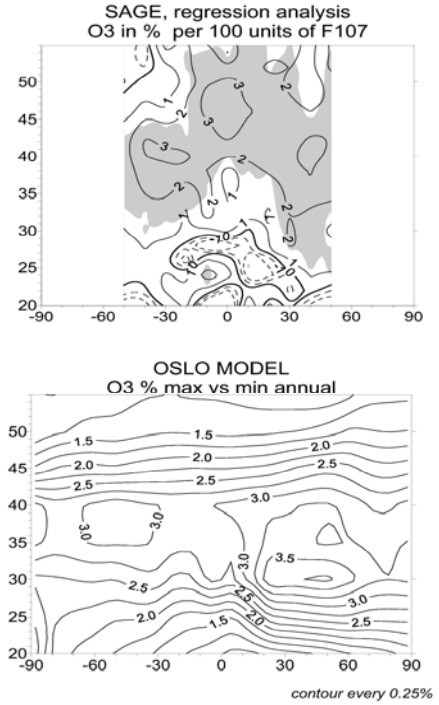

Figure 7.10 Percentage increase in ozone from solar min to max. Top: estimated from SAGE data. Bottom: estimated by a 2D model. (SOLICE, 2004).

Solar activity is manifest in not only variations in output of solar electromagnetic radiation but also in a range of other parameters. One of these is the occurrence and severity of coronal mass ejections which result in the emission of energetic particles, some of which reach the Earth. The highest energy particles penetrate well into the stratosphere and affect the chemical composition of the atmosphere. Precipitating electrons and solar protons affect the nitrogen oxide budget of the middle atmosphere through ionization and dissociation of nitrogen and oxygen molecules. NO catalytically destroys ozone, as discussed above, and reductions in ozone concentration may occur down to the middle stratosphere for a particularly energetic event (Jackman et al, 2001). As the solar particles follow the Earth's magnetic field lines these effects have greatest initial impact at high latitudes but ozone depletion regions may propagate downwards and equatorwards over the period of a few weeks. It is interesting to note that the effect of energetic particle events on ozone is in the opposite sense to that of enhanced ultraviolet irradiance. As particle events are more likely to occur when the Sun is in an active state the combined effect on ozone may be complex in its geographical, altitudinal and temporal distribution.

7.4. Clouds

To date no GCM simulations have been carried out attempting to simulate the proposed effects of galactic cosmic rays on cloud production. This is likely due to several factors: firstly GCMs, in general, include no representation of any ionisation effects whatsoever; secondly, model cloud prediction schemes are highly parameterised and tuned so not easily

adapted to different scenarios and thirdly, details of the proposed mechanisms have yet to be established so that any representation would necessarily be uncertain. GCMs have, however, been used to study the indirect effects of aerosol particles *viz.* (i) the increase in numbers of cloud condensation nuclei and subsequent decrease in mean droplet size and (ii) the increase in cloud lifetime resulting from the resulting suppression of precipitation. Thus a parameterisation of GCR effects would be feasible should their effects on cloud condensation nuclei become better known.

A few GCM studies have looked at the impact of variations in solar irradiance on clouds and precipitation. In general signals are very difficult to detect in such highly variable parameters but the modelling study of Meehl et al (2003) suggests that in the relatively cloud-free regions of the oceanic subtropics the surface energy flux is greater during periods of higher solar activity and that this drives stronger Hadley and Walker cells; van Loon et al (2004) find the same signal in NCEP Reanalysis data for the northern hemisphere summer. This result, however, is at odds with the Hadley cell weakening found by Haigh (2003) and Gleisner and Thejll (2003) also in NCEP data. This apparent disparity, which may be due to seasonal effects or merely a lack of statistical reliability in the analyses, remains to be resolved.

7.5. Modes of variability

Labitzke and van Loon (1992) found a link between solar activity, the QBO and the spring breakdown of the winter polar stratospheric vortex such that during the QBO East phase enhanced solar activity results in a colder vortex and a later breakdown while in the West phase the opposite seems to hold, though with less robustness The final warming of the winter polar stratosphere is brought about by upward-propagating planetary scale waves which are continually produced in the troposphere through the effects of topography or land-sea temperature contrasts. The upward propagation of the waves is determined by the thermodynamic structure of the stratosphere and Kodera (1995) has argued that a modification of the state of the stratosphere, such as induced by the absorption of enhanced solar UV radiation, will modify the wave propagation and result in the winter polar anomalies shown in Figure 7.7. Matthes et al (2004) have succeeded in simulating some of this response to solar UV, although in a model in which the QBO has to be forced by relaxation back to a zonal wind climatology.

It is possible that the effects of this wave-mean flow interaction can propagate downwards into the troposphere so that solar heating of the upper stratosphere might influence the state of the late winter troposphere. Rind et al (2002) present the results from GCM runs which also simulate the combined effects of solar variability and the QBO. Their results show that in the QBO East phase enhanced solar activity produces a positive AO anomaly, while the opposite (but smaller) effect is seen in the West phase. This is consistent with the Labitzke and van Loon (1992) anomalies in polar vortex temperatures extending down from the stratosphere. In another GCM study Shindell et al (2001) have suggested that the negative phase of the NAO may have been dominant during of the Maunder Minimum period of low solar activity.

The modelling and data studies are converging on a consistent picture. Details of the mechanisms involved need to be ascertained but it does appear that there are links between solar variability, the QBO and the winter high latitude circulations that can be simulated, at least qualitatively, by global climate models.

Published links between ENSO are solar variability are rather less robust but one recent study (Mann et al 2005) using a simplified climate model has found that both volcanic and solar

forcing are needed to produce a realistic simulation the mean and variability of El Niño over the past millennium.

8. Conclusions

Climate models have become a mainstay of atmospheric research. By numerical integration of the equations of motion they make it possible both to simulate current climate and also to assess the impacts of factors potentially involved in climate change. They are remarkably successful in the representation of the large scale features of the general circulation of the atmosphere, reproducing the major wind patterns, storm tracks, cloud patterns, precipitation and drought regions, and their seasonal variations. They also produce reasonable simulations of the monsoons and El Niño events. Where they are less successful is in representing some more local and regional events such as the timing of the diurnal maximum in tropical convection.

Due to the non-linearity of the coupled dynamical equations and the complexity of the physical processes involved, approximations are unavoidable in the construction of GCMs. Constraints are also imposed by limitations in the availability of computer power. Thus compromises have to be made between, for example, an increase in the grid resolution or an improvement in the representation of convection. The approximations include those required in the discrete representation of continuous functions, the representations of radiative transfer, cloud prediction, cloud-radiation interactions, sub-gridscale processes and ocean-atmosphere interactions. In many cases the underlying physics is well-known and the problem is to construct an accurate parameterisation; in others, such as details of cloud-aerosol interactions, physical understanding is incomplete and representations must largely rely on relationships derived empirically from observations. In the latter case it is not clear that relationships derived under one set of circumstances will necessarily apply to other situations.

Simulating the influence of solar variability on climate requires a knowledge of both the forcing factors and the mechanisms by which they influence the ocean-atmosphere system. Furthermore, statistically robust signals in atmospheric observations need to be available to assess the success of the model results. Advances are being made in all these areas but there remain several gaps in understanding. In terms of modelling the lower atmosphere these include (at least) the influence of solar ultraviolet radiation on stratospheric ozone and temperatures, any influence on tropospheric chemistry, the mechanisms of coupling between the upper and lower stratosphere including links with the QBO, mechanisms of stratosphere-troposphere coupling and details of any influence of atmospheric ionisation by cosmic rays on the supply of cloud condensation nuclei.

References

Andrews DG 2000 An Introduction to Atmospheric Physics. CUP

Baldwin, M.P., L.J. Gray, T.J. Dunkerton, K. Hamilton, P.H. Haynes, W.J. Randel, J.R. Holton, M.J. Alexander, I. Hirota, T. Horinouchi, D.B.A. Jones, J.S. Kinnersley, C. Marquardt, K. Sato, and M. Takahashi 2001 The Quasi-Biennial Oscillation. *Rev.Geophys.*, **39**, 179-229.

Baldwin MP, Dunkerton TJ 2001 Stratospheric harbingers of anomalous weather regimes. *Science*, **294**, 581-584.

Butchart N, Scaife AA, Austin J, Hare SHE, Knight JR 2003 Quasi-biennial oscillation in ozone in a coupled chemistry-climate model. *J.Geophys.Res.*, **108**, art. no. 4486.

Crowley TJ Causes of climate change over the past 1000 years. *Science*, **289** 270-277.

Dickinson RE 1975 Solar variability and the lower atmosphere. *Bull. Am. Meteorol. Soc.*, **56**, 1240-1248.
Gleisner H and P Thejll 2003 Patterns of tropospheric response to solar variability. *Geophys Res Lett,* **30,** art. No. 1711 .
Gray LJ, Crooks SA, Pascoe, C and Sparrow S 2005 Solar and QBO influences on the timings of stratospheric sudden warmings. *J.Atmos.Sci.* in press.
Haigh J D 1994 The role of stratospheric ozone in modulating the solar radiative forcing of climate. *Nature*, **370**, 544-546.
Haigh J D 1996 The impact of solar variability on climate. *Science*, **272**, 981-984.
Haigh J D 1999 A GCM study of climate change in response to the 11-year solar cycle. *Quart.J.Roy.Meteorol.Soc.*, **125**, 871-892.
Haigh, J D 2003 The effects of solar variability on the Earth's climate. *Phil. Trans. Roy. Soc A.*, **361**, 95-111.
Haigh J D, M Blackburn and R Day 2005 The response of tropospheric circulation to perturbations in lower stratospheric temperature. *J. Clim.*, in press.
Harrison RG and KS Carslaw 2003 Ion-Aerosol-Cloud Processes in the Lower Atmosphere. *Rev. Geophys.*, **41**,3.
Holton JR 1992 An Introduction to Dynamic Meteorology. AP
Houghton JT 1977 The Physics of Atmospheres. CUP
IPCC 2001 Climate Change 2001: The Scientific Basis. CUP.
Jackman CH, McPeters RD, Labow GJ, Fleming EL, Praderas CJ and Russell JM 2001 Northern Hemisphere atmospheric effects due to the July 2000 solar proton event *Geophys Res Lett*, **28**, 2883-2886.
Jacobson MZ 1999 Fundamentals of Atmospheric Modeling. CUP.
Kiehl J T and K E Trenberth 1997 Earth's annual global mean energy budget *Bull. Am. Meteorol. Soc.*, **78**, 197-208.
Kodera K 1995 On The Origin And Nature Of The Interannual Variability Of The Winter Stratospheric Circulation In The Northern-Hemisphere. *J.Geophys.Res.,* **100**, 14077-14087.
Labitzke K and H van Loon 1992 On The Association Between The QBO And The Extratropical Stratosphere *J.Atmos.Terrest.Phys.*, **54**, 1453-1463.
Latif M, Dommenget D, Dima M and Grotzner A 1999 The role of Indian Ocean sea surface temperature in forcing east African rainfall anomalies during December-January 1997/98. *J.Clim.*, **12**, 3497-3504.
Lean J 1991 Variations In The Sun's Radiative Output. *Rev Geophys,* **29,** 505-535.
Ludlam FH 1980 Clouds and storms: the behavior and effect of water in the atmosphere. Penn State Press
Mann ME, MA Cane, SE Zebiak and A Clement 2005 Volcanic and solar forcing of the tropical Pacific over the past 1000 years. *J.Clim.*, **18**, 447-456.
Marsh ND and H Svensmark 2000 Low cloud properties influenced by cosmic rays *Phys Rev Lett* **85**, 5004-5007.
Matthes K et al 2003 GRIPS intercomparison project solar experiments: initial results. *Papers in Meteorol. Geophys.*, **54**, 71-90.
Matthes K, U Langematz, LJ Gray, K Kodera and K Labitzke 2004 Improved 11-year solar cycle in the Freie Universität Berlin climate middle atmosphere model (FUB-CMAM). *J.Geophys.Res.*, **109**, D06101.
Meehl GA, WM Washington, TML Wigley, JM Arblaster and JM Dai 2003 Solar and greenhouse gas forcing and climate response in the 20th century. *J.Clim.*, **16**, 426-444.

Nakajima T and MD King 1990 Determination Of The Optical-Thickness And Effective Particle Radius Of Clouds From Reflected Solar-Radiation Measurements .1. Theory *J Atmos Sci,* **47** , 1878-1893.

Rind D, P Lonergan, NK Balachandran and D Shindell 2002 2 x CO_2 and solar variability influences on the troposphere through wave-mean flow interactions. *J.Meteorol.Soc.Jap.*, **80**, 863-876.

Robock A 2001 Stratospheric forcing needed for dynamical seasonal prediction *B.A.Meteorol.Soc.*, **82**, 2189-2192.

Shindell DT, Miller RL, Schmidt GA and Pandolfo L 1999a Simulation of recent northern winter climate trends by greenhouse-gas forcing. *Nature,* **399**, 452-455.

Shindell DT , D Rind, N Balachandran, J Lean and P Lonergan 1999b Solar cycle variability, ozone and climate. *Science*, **284**, 305-308.

Shindell DT, Schmidt GA, Mann ME, Rind D and Waple A 2001 Solar forcing of regional climate change during the Maunder Minimum. *Science,* **294**, 2149-2152.

Slingo JM 1987 The development and verification of a cloud prediction scheme for the ECMWF model. *Q.J.Roy.Meteorol.Soc.*, **113**, 899-927.

SOLICE 2004 Final Report of European Community Framework Programme 5 project Solar Influences on Climate and the Environment.

Stott PA, Jones GS and Mitchell JFB 2003 Do models underestimate the solar contribution to recent climate change? *J.Clim.*, **16**, 4079-4093.

Strobel DF 1978 Parameterization of the atmospheric heating rate from 15 to 120 km due to O_2 and O_3 absorption of solar radiation, *J. Geophys. Res*., **83**, 6225-6230.

Tinsley BA 2000 Influence of the solar wind on the global electric circuit and inferred effects on cloud microphysics, temperature and dynamics in the troposphere. *Space Sci. Rev*., **94**, 231-258.

van Loon H, Meehl GA and Arblaster JM 2004 A decadal solar effect in the tropics in July-August J.Atmos.Sol.-Terrest.Phys., **66**, 1767-1778.

Warner CD and McIntyre ME 2001 An ultrasimple spectral parameterization for nonorographic gravity waves. *J.Atmos.Sci.*, **58**, 1837-1857.

Yu F 2002 Altitude variations of cosmic ray induced production of aerosols: Implications for global cloudiness and climate. *J. Geophys. Res.*, **107**, 1118

Yu F and RP Turco 2001 From molecular clusters to nanoparticles: Role of ambient ionisation in tropical aerosol formation. *J. Geophys. Res.*, **106**, 4797-4814.